analytica

MDPI

Article

Reagent-Free Spectroscopic Assays for Arginase Activity for Heterogenic System

Igor D. Zlotnikov [1,2,*], Polina I. Novikova [2] and Elena V. Kudryashova [1,2,*]

[1] Laboratory of Targeted Therapy and Diagnostics, Central University, 7 Gasheka St., Moscow 123056, Russia
[2] Faculty of Chemistry, Lomonosov Moscow State University, Leninskie Gory, 1/3, Moscow 119991, Russia
* Correspondence: izlotnikov2003@yandex.ru (I.D.Z.); helenakoudriachova@yandex.ru (E.V.K.)

Abstract

Arginase is an enzyme of medical significance that plays a crucial role in research on macrophages, in the field of oncology, and serves as a biomarker in various areas. However, the current methods for assessing its activity rely on indirect, time-consuming colorimetric assays, which cannot provide real-time kinetic data in complex media. This is a critical aspect in biomedical research. To address this issue, we have developed two novel spectroscopic methods without the use of reagents, based on circular dichroism (CD) spectroscopy and attenuated total reflection Fourier transform infrared (ATR-FTIR) spectroscopy. The approach based on CD proved to be particularly effective in capturing the complete progress curve of arginine hydrolysis within a single measurement, with high sensitivity, enabling detection limits as low as 0.026 U/mL. Nonetheless, the use of CD is primarily restricted to homogeneous and optically transparent solutions. In contrast, ATR-FTIR allows for real-time monitoring of specific bands within the substrate and product (arginine and ornithine, respectively) in complex and non-transparent media such as cell cultures, without the need for sample preparation. This method enables us to measure arginase activity in a living culture of Lewis lung carcinoma cells (LLC1), where the liposomal form of arginase demonstrates a remarkable 6.4-fold increase in specific activity compared to the native enzyme.

Keywords: arginase; arginine deprivation therapy; circular dichroism; FTIR spectroscopy; enzyme kinetics; liposomal enzyme; thermal denaturation; secondary structure

Academic Editor: Marcello Locatelli

Received: 31 August 2026
Revised: 23 October 2026
Accepted: 25 October 2026
Published: 29 October 2026

Copyright: © 2026 by the authors. Licensee MDPI, Basel, Switzerland. This article is an open access article distributed under the terms and conditions of the Creative Commons Attribution (CC BY) license.

1. Introduction

L-Arginase (L-arginine amidinohydrolase, EC 3.5.3.1) catalyzes the Mn^{2+}-dependent hydrolysis of L-arginine to L-ornithine and urea, the terminal cytosolic step of the hepatic urea cycle [1–9]. Two isoforms are expressed in mammals: cytosolic arginase-1 (Arg1), highly expressed in hepatocytes and central to ureagenesis and ammonia detoxification, and mitochondrial arginase-2 (Arg2), first identified in kidney [10], which supplies L-ornithine, polyamines, proline, and glutamate to extrahepatic tissues [2,7]. Despite differing subcellular localization and tissue specificity, the two isoforms share ~60% sequence identity and a conserved catalytic machinery: a binuclear Mn^{2+} center coordinated by His-101, Asp-124, His-126, Asp-128, Asp-232, and Asp-234 (human Arg1 numbering) [4]. Both isoforms assemble as homotrimers (Arg1) or, after mitochondrial import and N-terminal presequence cleavage, a topologically equivalent homotrimer (Arg2), with nearly

identical inter-subunit contacts and active-site geometry at the monomer level [11]. Each monomer adopts an α/β fold topologically related to the Rossmann fold—a central eight-stranded parallel β-sheet flanked by α-helices on both faces [12]. Catalysis proceeds through nucleophilic attack of a Mn^{2+}-bridging hydroxide ion on the guanidinium carbon of L-arginine, generating a tetrahedral intermediate that is electrostatically stabilized by the binuclear Mn(II) center; His-141-mediated proton transfer then cleaves the C–N bond, releasing urea and leaving L-ornithine [3,13,14]. The reaction is thermodynamically essentially irreversible ($\Delta G° \approx -15$ kcal/mol) [3]. Human arginases display strict metal specificity: substitution of Mn^{2+} by Co^{2+}, Ni^{2+}, or other bivalent cations abolishes native-metal catalytic activity outright, although, notably, Co^{2+}-substituted human Arg1 has been engineered into a distinct, clinically advanced high-activity variant with a shifted pH optimum (pegzilarginase; Table 1) [1,11].

Arginase has gained significant interest as a therapeutic protein beyond nitrogen homeostasis. Many cancers, such as hepatocellular carcinoma, melanoma, and sarcomas, are arginine-auxotrophic due to insufficient argininosuccinate synthetase or lyase activity. Exogenous arginase depletes extracellular arginine, starving these tumor cells, which arrest proliferation and undergo non-apoptotic cell death [5,15]. Normal tissues with arginine-recycling capacity are spared. Engineered arginase biologics have been developed, as summarized in Table 1.

Table 1. Comparative kinetic parameters of arginase variants at optimal and physiological conditions.

Enzyme	Origin	pH Optimum	Activity at pH 7.4 (% of Max) *	K_M at pH 7.4 (mM)	k_{cat} at pH 7.4 (s^{-1})	k_{cat}/K_M at pH 7.4 ($mM^{-1}s^{-1}$)	Delivery Profile & Therapeutic Significance	Ref.
Bovine ARG	Bovine liver	9.4–9.5	~10–15%	~2–3.4	~20–30	~5–10	Historical reference model; strong structural stability but high immunogenicity; poor catalytic efficiency at blood pH limits direct clinical use	[3,16]
Rat ARG1	Rat liver	9.4–9.7	~10–15%	~1.0	~25–35	~4–10	Crucial preclinical in vivo model; baseline for macrophage-related immune response studies; native activity at pH 7.4 suppressed	[10]
Human ARG1 (native, Mn^{2+})	Human (native)	~9.0	~10–15%	2.3 ± 0.3	300 ± 12	129 ± 20	Gold standard for targeted arginine depletion; severely limited by rapid clearance, proteolysis, and low systemic activity at physiological pH	[5,16]
BCT-100	PEGylated hARG1 (Mn^{2+})	9.0	~10–15%	~2.0–4.0	~25–30	~8–15	PEGylation increases half-life and shields from proteases, but does not solve the fundamental low catalytic efficiency at blood pH	[17]
Pegzilarginase (AEB1102)	Co^{2+}-substituted PEG-hARG1	~7.5	100% (by design)	0.19 ± 0.04	240 ± 14	1270 ± 330	Co^{2+}-for-Mn^{2+} substitution lowers K_M and shifts the pH-dependence, boosting k_{cat}/K_M ~10-fold at pH 7.4 relative to the native Mn^{2+} enzyme	[18]

LipoARG (this study)	Liposomal formulation	9.0–9.5	Locally enhanced	~2–3	Preserved core activity	Modulated by bilayer kinetics	Lipid bilayer protects the enzyme corona and alters substrate diffusion; enables cellular uptake and localized action within the tumor microenvironment	this work

* Estimated percentage of residual catalytic activity at physiological pH (7.4) relative to the enzyme's absolute maximum activity at its alkaline pH optimum (~9.5), except for the Human ARG1 and Pegzilarginase rows, where k_{cat}/K_M values are direct literature measurements at pH 7.4 [18].

While engineering strategies such as metal substitution (e.g., Co^{2+}-substituted pegzilarginase) have been employed to enhance catalytic efficiency, they introduce potential safety and efficacy concerns. Specifically, non-native metal substitution raises issues of potential heavy-metal toxicity upon in vivo release.

An alternative and highly promising strategy is to preserve the native Mn^{2+} active site but encapsulate the enzyme within a lipid-based nanocarrier (bottom row, Table 1). This approach is particularly relevant given that the tumor interstitium is significantly more acidic than physiological blood, which further suppresses the systemic activity of the free enzyme. Liposomal formulations provide an excellent platform to overcome these biological barriers. They can be engineered for selective accumulation in tumor tissues and liver metastases, while their lipid bilayers facilitate direct intracellular delivery of the biocatalyst through membrane fusion, directly targeting cancer cells. Developing various specialized formulations is critical for achieving this selective accumulation; however, rationally designing and optimizing these liposomal platforms requires continuous, precise measurement of the encapsulated enzyme's activity. Therefore, developing a high-throughput, reagent-free analytical method capable of functioning in complex, turbid lipid media is an urgent prerequisite for advancing these targeted nanocarriers.

Beyond its therapeutic relevance, arginase is increasingly recognized as a bioanalytical marker in its own right—its activity serves as a diagnostic indicator in hepatic, cardiovascular, and immune-related pathologies, and as a critical process parameter during biopharmaceutical production and formulation control. A second bottleneck in arginase research and the central analytical motivation of this study is the absence of simple, direct, real-time assays for catalytic activity. The great majority of published arginase assays fall into three classes: (i) residual-substrate colorimetric assays (Sakaguchi-type reactions of L-arginine with 8-hydroxyquinoline/hypobromite [19], or with p-nitrophenylglyoxal [20]); (ii) product-based colorimetric assays, most commonly detection of urea via the diacetyl monoxime reaction [21,22] or detection of L-ornithine via ninhydrin (Chinard reaction) [23,24]; and (iii) coupled enzymatic/electrochemical schemes, such as the arginase→urease→glutamate dehydrogenase cascade (Ozer method) [25] or potentiometric/ion-selective-electrode and pH-stat assays that rely on urease-generated ammonium [26]. All of these approaches are indirect: they require a reaction-stopping step, an auxiliary chromogenic or enzymatic reagent, and/or elevated temperature for color development, and none of them reports the reaction as it proceeds in real time on the native substrate/product pair. Spectroscopic methods that directly exploit the intrinsic optical signatures of L-arginine and L-ornithine—far-UV absorbance/CD and IR (ATR-FTIR)—have been used to monitor other enzymatic reactions in real time and in optically complex media such as blood and plasma [27–29], but, to our knowledge, have not previously been described for arginase.

To demonstrate the practical value of this analytical approach for formulation testing, we apply it to a concrete case study: a liposomal form of arginase-1 (lipo-ARG), using the new native-substrate assays to quantitatively evaluate how encapsulation affects the

enzyme's catalytic efficiency at its alkaline pH optimum. Finally, to comprehensively characterize this delivery system, far-UV CD spectroscopy—established above as a real-time activity probe—is additionally applied in its classical structural role, acquiring temperature-resolved CD thermograms of free vs. liposomal arginase. Rather than reducing this to a single "denaturation" endpoint, these thermograms are used to resolve the underlying structural transitions—conformational destabilization, aggregation, cofactor dissociation, subunit dissociation, and the specific unfolding mechanism—and to determine how liposomal formulation modulates each of these processes. By translating raw ellipticity data into quantitative, temperature-resolved metrics of structural retention and deriving van't Hoff thermodynamic parameters, we intend to determine whether liposomal encapsulation predominantly enhances intrinsic conformational stability, modulates the local catalytic microenvironment, or operates through a combination of both mechanisms.

For bioanalytical chemistry, these results are expected to deliver a broadly transferable toolkit: reagent-free, real-time spectroscopic assays extendable to other enzymes lacking convenient native chromophores, together with a structural-thermodynamic framework for assessing how nanocarrier encapsulation affects biocatalyst stability and function.

2. Materials and Methods

2.1. Reagents and Chemicals

L-Arginine (Sigma-Aldrich, St. Louis, MO, USA, BioUltra, ≥99.5%) and L-ornithine monohydrochloride (Sigma-Aldrich, ≥99%) were used as the substrate and reference product, respectively. L-*α*-phosphatidylcholine was purchased from Sigma-Aldrich (St. Louis, MO, USA), and cardiolipin was obtained from Avanti Polar Lipids (Alabaster, AL, USA).

2.2. Enzyme Source and Metal Activation

Lyophilized arginase-1 from bovine liver (Leap Chem Co., Ltd., Hong Kong; CAS No. 9000-96-8, SDS-PAGE purity ≥90%, specific activity 127 U/mg, retaining ≥90% activity after 7 days at 37 °C) was employed for all enzymatic assays. Because the catalytic activity of arginase strictly depends on a binuclear manganese cluster, the enzyme was subjected to a specific metal pre-activation protocol prior to all experiments to ensure the full population and stabilization of the active site. Briefly, the 1 mg/mL enzyme was incubated in the presence of 1 mM $MnCl_2$ at 55 °C for 20 minutes. Following this activation step, the enzyme preparation was immediately utilized for either liposome encapsulation (Section 2.3) or free-enzyme continuous kinetic assays.

2.3. Preparation of Liposomal Arginase (Lipo-ARG)

The Mn-activated enzyme was encapsulated in phospholipid vesicles composed of phosphatidylcholine and cardiolipin at an 80:20 mol% ratio. These liposomes were prepared via the thin-lipid-film hydration method, with the lipid and pre-activated enzyme combined at a 3:1 mass ratio (*w*/*w*) during the hydration step. Sequential membrane extrusion, first through a 400 nm and subsequently through a 200 nm polycarbonate membrane, was employed to narrow and homogenize the vesicle size distribution.

Hydrodynamic diameter, polydispersity, and zeta potential measurements were conducted using a Zetasizer Nano S (Malvern Instruments, Worcestershire, UK) equipped with a 4 mW He–Ne laser (633 nm) at a fixed scattering angle of 173° and a temperature of 25 °C. Experimental data processing and analysis were performed using Zetasizer Software (v. 8.02). To determine the encapsulation efficiency, the unencapsulated arginase

was separated from the liposomal fraction via dialysis using a 300 kDa molecular weight cutoff (MWCO) cassette. The free protein in the dialysate was subsequently quantified by measuring its intrinsic tryptophan fluorescence. To ensure a rigorous mass balance, this quantification was orthogonally validated using ATR-FTIR spectroscopy. The absolute protein distribution was confirmed by directly integrating the area of the protein-specific Amide I (~1650 cm^{-1}) and Amide II (~1550 cm^{-1}) vibrational bands in both the purified liposomal fraction and the unencapsulated dialysate.

2.4. Real-Time Activity Assay Using CD Spectroscopy

CD measurements were performed on a Jasco J-815 CD spectrometer (JASCO, Tokyo, Japan) with a thermostated cell. Far-UV CD and absorbance spectra (180–250 nm) of 1–20 mM L-arginine and L-ornithine in water were first recorded to select diagnostic analytical wavelengths. Absorbance at 200 nm and CD ellipticity at 205 nm were selected as the analytical wavelengths for kinetic monitoring (2-min step). Reactions were initiated by adding arginase (final concentration 0.001–0.1 mg/mL) to 1–20 mM L-arginine in water (self-buffered at pH ≈ 9.1 by the substrate itself and 1 mM CHES) in a 1-mm-pathlength quartz cuvette at 37 °C, and the decay of the arginine signal/rise in the ornithine signal was followed continuously for free arginase and lipo-ARG. At the experimental substrate concentrations (1–30 mM), the free-base amino group of L-arginine inherently shifts the solution pH to approximately 9.1, which closely approximates the enzyme's alkaline pH optimum (~9.5). To ensure strict pH stability across all experiments without introducing spectral interference in the targeted CD and FTIR windows, 1 mM CHES was included in all assay solutions. This approach circumvents the need for high concentrations of conventional buffer salts, whose intrinsic vibrational and optical bands could otherwise obscure the monitored signals. To experimentally confirm the stability of this self-buffering system during the hydrolytic cleavage of the basic guanidinium group, the pH of the reaction mixtures was directly measured before enzyme addition and immediately following the completion of the kinetic monitoring. In all cases, the initial pH was established at 9.1±0.05, and the pH did not fluctuate by more than 0.1 units over the entire course of the reaction, definitively ruling out pH drift as a confounding factor in the kinetic or spectral analyses.

Using the mass-balance relation [Orn] = C_0(Arg) − [Arg], kinetic traces were converted into product-accumulation curves, and initial rates (v_0) were obtained from the slope of the initial linear segment.

Kinetic parameters were obtained by two independent routes. In the integrated (Walker–Schmidt) approach, the closed-form solution of the Michaelis–Menten rate equation,

$$K_M \times \ln([S]_0/[S]) + ([S]_0 - [S]) = V_{max} \cdot t, \quad (1)$$

was fit directly to the substrate-depletion time course [S](t) (with $[S]_0$ the initial arginine concentration), avoiding the need to differentiate noisy experimental traces to obtain instantaneous rates. As a cross-check, the same dataset was fit by numerical integration of the differential rate equation including linear competitive product inhibition by L-ornithine,

$$d[S]/dt = -V_{max} \cdot [S]/\{K_M \times (1 + [P]/Ki) + [S]\}, \quad (2)$$

with [P] = $[S]_0$ − [S] and *K*i the ornithine inhibition constant, solved numerically and fit to the experimental [S](t) trace by nonlinear least squares. During data processing, it was determined that the standard integrated equation without product inhibition (Equation (1)) resulted in poor approximation and systematic deviations at later reaction stages due to ornithine accumulation. Consequently, robust and statistically identifiable parameter

estimation was exclusively achieved using the numerical integration of the differential rate equation incorporating competitive product inhibition (Equation (2)). Therefore, all final kinetic parameters (V_{max}, K_M, and K_i) reported in the tables of this study were derived solely using this product-inhibition model.

2.5. Real-Time Activity Assay Using ATR-FTIR Spectroscopy

FTIR spectra were recorded on a Tensor 27 FTIR spectrometer (Bruker, Ettlingen, Germany) with an MCT detector (liquid-N_2-cooled) and a thermostated BioATR II cell (ZnSe single-reflection element, 37 °C, Huber thermostat). Reference spectra of 30 mM L-arginine and L-ornithine in water (self-buffered at pH ≈ 9.1 by the substrate itself and 1 mM CHES) (4000–850 cm^{-1}, 1 cm^{-1} resolution, 70 scans, background-subtracted) identified diagnostic bands. For kinetic runs, a 30-µL aliquot of L-arginine (1–30 mM) was applied to the ATR element and the reaction initiated by adding arginase; spectra were collected every 60 s for free arginase and liposomal arginase. In both datasets, the initial spectrum (0 min) shows the full-intensity guanidinium group (1675 cm^{-1}, ATR units normalized to 1.0), which progressively collapses into the single, ornithine-dominated envelope (maximum near 1600 cm^{-1}) as the reaction proceeds. This mutual spectral exclusivity of the 1630/1675 cm^{-1} guanidinium doublet (present only in arginine) defines the fundamental structural basis for FTIR kinetic monitoring. For rigorous quantitative analysis, the extreme high-frequency shoulder of this doublet, extending toward 1690 cm^{-1}, was specifically utilized for integration. This high-wavenumber region provides an optimal, interference-free analytical window for tracking substrate depletion because it remains completely unaffected by the overlapping emergence of the product's carboxylate band (~1605 cm^{-1}) or potential background fluctuations from the protein Amide I region. The 1690 cm^{-1} band-intensity changes over time were converted to product-formation curves, v_0 was obtained as above, and K_M V_{max} were extracted by the same integrated-kinetics and differential-equation (product-inhibition) approaches used for the CD assay.

2.6. Analytical Figures of Merit (LOD/LOQ)

One unit (U) of arginase activity is defined as the amount of enzyme required to catalyze the formation of 1 micromole of L-ornithine per minute at 37 °C and pH ~9.1 under substrate-saturating conditions.

To ensure a fully reproducible analytical framework, the limit of detection (LOD) and limit of quantification (LOQ) for all three spectroscopic modalities were calculated in accordance with standard IUPAC guidelines, based on the standard deviation of the blank response and the slope of the calibration sensitivity. The specific equations utilized were LOD = 3 × (SD_blank/S); LOQ = 10 × (SD_blank/S), where SD_blank is the standard deviation of the instrumental baseline noise, and S is the slope (analytical sensitivity).

For each modality, SD_blank was robustly determined from 15 successive signal measurements of the enzyme-free substrate blank (20 mM or 30 mM L-arginine) under exact assay conditions (37 °C). The sensitivity slope (S) was derived from the highly linear initial phase of the product accumulation curves (where the change in optical signal is strictly proportional to product formation) and converted into activity units (U/mL) using the respective molar absorption coefficients and molar ellipticities. For UV absorbance at 200 nm, the applied molar absorption coefficients for L-arginine and L-ornithine were 2650 and 750 $M^{-1}{\cdot}cm^{-1}$, respectively (difference coefficient 1900 $M^{-1}{\cdot}cm^{-1}$).

Furthermore, the analytical precision of the developed continuous methodology was evaluated. Intra-day (within-run) precision was assessed by measuring the activity of a standard free arginase preparation (0.02 mg/mL) in three independent technical replicates on the same day. Inter-day precision was evaluated by repeating this triplicate analysis across three consecutive days. For all three modalities (CD, UV absorbance, and ATR-

FTIR), the calculated relative standard deviations (RSDs) for both intra-day and inter-day precision were consistently below 5%. This confirms the high operational stability and excellent analytical reproducibility of the proposed reagent-free platform

2.7. Thermal Denaturation and Secondary-Structure Analysis

Far-UV CD spectra (200–260 nm) of free arginase and lipo-ARG (2 mg/mL) were recorded from 20 to 80 °C in 10 °C increments, alongside the corresponding UV absorbance spectra. To precisely monitor the structural transition from the native α/β fold to an unfolded state while compensating for potential temperature-induced baseline drift and liposomal light scattering, a differential analytical approach was utilized. Rather than relying on a single wavelength, the structural shift was quantified using the difference in ellipticity between the random coil diagnostic region (200 nm) and the α-helix diagnostic minimum (222 nm), defined as $\Delta\theta = \theta_{200} - \theta_{222}$. As thermal denaturation progresses, the unfolding of α-helices reduces the negative signal at 222 nm, while the concomitant accumulation of random coil structures significantly increases the negative signal at 200 nm. This simultaneous bidirectional signal change maximizes the sensitivity of the $\Delta\theta$ parameter to the unfolding event. To express secondary-structure loss independently of the absolute CD amplitudes of the two formulations, each dataset was normalized to its own native (20 °C) and heat-denatured (80 °C) endpoints to determine the unfolded fraction:

$$\theta_\text{unfolded}(T) = [\Delta\theta(20\ °C) - \Delta\theta(T)]/[\Delta\theta(20\ °C) - \Delta\theta(80\ °C)].$$

The apparent melting temperature T_m and unfolding thermodynamics (ΔH, ΔS) were derived from a van't Hoff plot of $R \cdot \ln K$ (where $K = \theta_\text{unfolded}/(1 - \theta_\text{unfolded})$) against $1/T$, fitted to the linear equation $R \cdot \ln K = -\Delta H/T + \Delta S$.

The derived parameters (T_m, ΔH, and ΔS) are explicitly defined and reported throughout this study as apparent, empirical descriptors. Rather than serving as absolute thermodynamic state functions, these apparent quantities are used strictly as a robust comparative mathematical framework to quantitatively evaluate the relative structural resilience of the free versus encapsulated enzyme formulations under identical thermal stress.

2.8. Kinetics of Irreversible Thermal Inactivation

To determine the kinetics of irreversible thermal inactivation, samples of free arginase and liposomal arginase (lipo-ARG) were incubated in a thermostated water bath at constant temperatures of 55 °C and 70 °C. At predefined time intervals (ranging from 0 to 60 min), aliquots were withdrawn and immediately transferred to an ice bath. This rapid cooling step was strictly employed to quench the thermal denaturation process and prevent any further conformational degradation prior to analysis. Following the ice-cooling step, the residual catalytic activity A of each aliquot was measured using the developed continuous far-UV CD assay at 37 °C, tracking the ellipticity decay at 205 nm. To ensure zero-order kinetic conditions with respect to the substrate, all inactivation measurements were conducted at a saturating L-arginine concentration of 15 mM. The residual activity was expressed as a ratio (A/A_0), where A_0 represents the absolute initial activity of the corresponding unheated control sample. The apparent first-order inactivation rate constants k_{in} were derived from the slopes of the initial linear phase of the semi-logarithmic plots representing $\ln(A/A_0)$ as a function of incubation time. The activation energy of inactivation Ea was subsequently calculated from these temperature-dependent rate constants using the Arrhenius equation.

2.9. In Vitro Cellular Association and Activity Assay

To evaluate the cellular binding and functional retention of the arginase formulations, murine Lewis lung carcinoma (LLC1) cells (ATCC CRL-1642) were utilized as a representative solid tumor in vitro model. The LLC1 cells were incubated with equivalent initial doses of either free arginase or liposomal arginase for 6 h at 37 °C under standard culture conditions. Following the incubation period, the cell suspensions were washed twice with phosphate-buffered saline (PBS) via centrifugation to rigorously remove any unassociated or weakly bound enzyme from the bulk medium. The catalytic activity of the remaining firmly cell-associated arginase fractions was subsequently quantified using the continuous ATR-FTIR spectroscopic assay under standard substrate-saturating conditions (pH ~9.1, 37 °C). To ensure accurate comparative evaluation, the specific activity of the cell-bound fraction was mathematically normalized and expressed as units per milligram of the initially added enzyme (U/mg).

2.10. Data Processing and Statistical Analysis

The quantitative deconvolution of the protein secondary structure (estimating the percentage fractions of alpha-helices, beta-sheets, beta-turns, and random coils) was performed by processing the far-UV CD spectra through the CDNN secondary structure analysis software (Version 2.1). All analytical measurements, including enzymatic kinetic assays, dynamic light scattering, and thermal denaturation experiments, were performed using n = 3 independent technical replicates (independent aliquots and instrumental runs sampled from the prepared batch). Experimental data in the text and figures are presented as the arithmetic mean ± SD. Kinetic and thermodynamic modeling, including the extraction of Michaelis–Menten parameters via non-linear regression of the integrated rate equations, was executed using OriginPro software (Version OriginPro 2024). The statistical errors reported for the extracted kinetic parameters in the tables represent the standard errors of the nonlinear regression fits, reflecting their 95% confidence intervals. To validate the robustness of the nonlinear models beyond a simple coefficient of determination R^2, we employed rigorous residual diagnostics; acceptable fits were required to exhibit a random, zero-centered distribution of residuals without systematic geometric bias. Inferential statistical analysis to compare the properties of the free and liposomal formulations (such as catalytic constants and residual activities) was performed using an unpaired, two-tailed Student's *t*-test. Differences were considered statistically significant at a *p*-value of <0.05.

3. Results

3.1. Catalytic Mechanism of Arginase and Rationale for Label-Free Spectroscopic Monitoring

Arginase is a metalloenzyme that catalyzes the final step of the urea cycle, specifically the hydrolysis of the semi-essential amino acid L-arginine to yield L-ornithine and urea. As depicted in Figure 1, the active site of arginase features a highly conserved binuclear manganese cluster that is essential for its catalytic function. The enzymatic cycle is initiated by the binding of L-arginine in the active site cavity, where it is optimally positioned by a network of hydrogen bonds.

The core catalytic event involves a metal-bridging hydroxide ion, which is coordinated by the two manganese ions and further stabilized by interactions with surrounding conserved residues, notably Asp-128. This hydroxide ion acts as a potent nucleophile, attacking the central carbon atom of the planar guanidinium group of L-arginine. This nucleophilic attack generates a tetrahedral intermediate. Subsequently, dynamic proton transfer events—facilitated by the neighboring His-141 and Glu-277 residues—trigger the collapse of this intermediate. This leads to the cleavage of the C–N bond, the release of L-

ornithine and urea, and the eventual regeneration of the nucleophilic hydroxide via the binding and deprotonation of a new water molecule.

The biochemical conversion of L-arginine to L-ornithine involves a profound structural and electronic change: the loss of the large, highly basic, and resonance-stabilized guanidinium group, which is replaced by a simple primary amine in the product. This specific structural transformation provides an ideal foundation for real-time, reagent-free reaction monitoring. Because the substrate and the primary product possess significantly different optical and vibrational properties, we hypothesized that their distinct far-UV CD and FTIR spectroscopies could be applied to directly track the hydrolytic kinetics in real-time, without the need for coupled enzymatic assays or exogenous chemical labels.

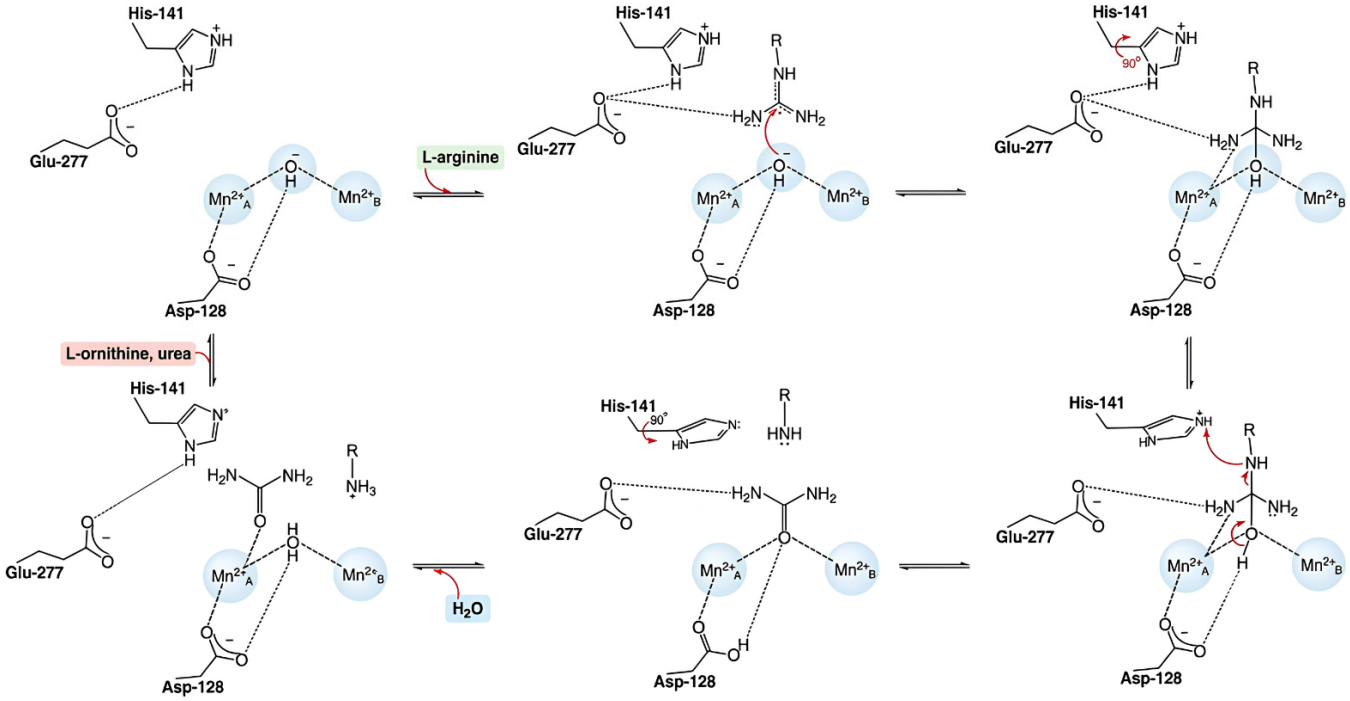


Figure 1. Proposed catalytic mechanism of L-arginine hydrolysis by arginase. The reaction occurs at the active site featuring a binuclear manganese cluster (Mn^{2+}_A and Mn^{2+}_B) and involves key conserved residues (Asp-128, His-141, and Glu-277). The mechanism proceeds via the nucleophilic attack of a metal-bridging hydroxide ion on the guanidinium group of L-arginine, leading to the formation of a tetrahedral intermediate, followed by the subsequent release of L-ornithine and urea. Adapted from [4].

3.2. Spectroscopic Differentiation of the Substrate and Product and Assignment of Spectral Transitions

To establish the foundation for a reagent-free kinetic assay, the individual optical properties of the substrate (L-arginine) and the product (L-ornithine) were characterized in detail. Figure 2 presents the far-UV circular dichroism (CD) and UV absorption spectra of 10 mM aqueous solutions of both amino acids, revealing the profound spectral changes induced by the cleavage of the guanidinium group.

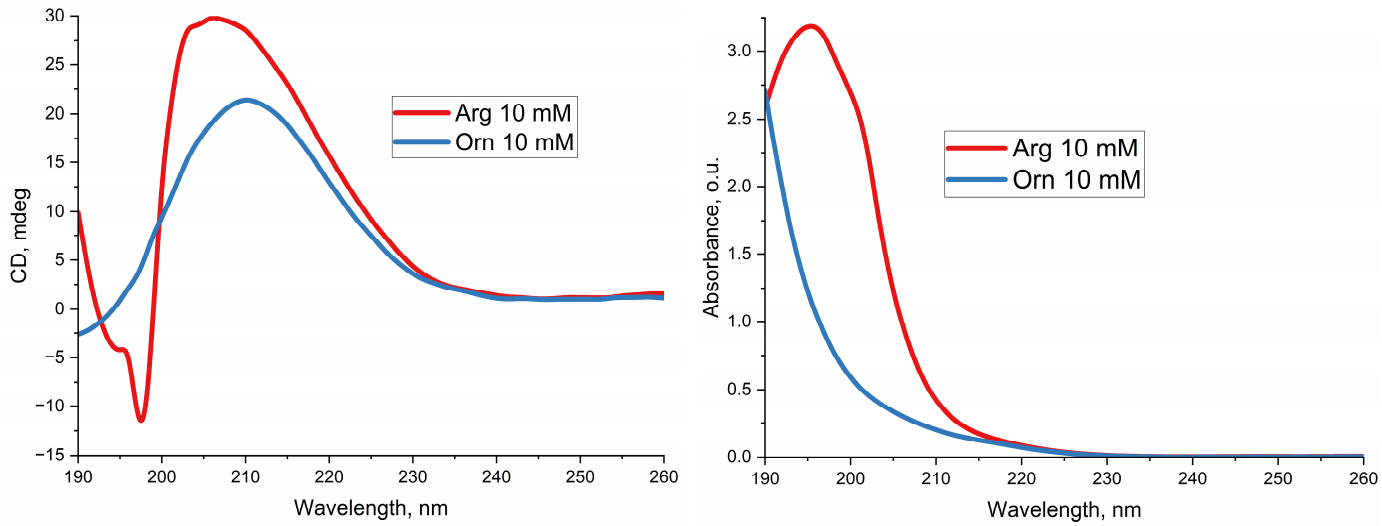


Figure 2. Spectroscopic characterization of the substrate and the product. (**a**) Circular dichroism (CD) and (**b**) UV absorption spectra of 10 mM L-arginine (red line) and 10 mM L-ornithine (blue line) in aqueous solutions.

The UV absorption spectra (Figure 2b) demonstrate a pronounced differentiation driven by the specific chromophores present in each molecule. L-arginine exhibits a broad absorption profile that maintains high signal intensity up to approximately 210 nm. This extended absorbance is primarily attributed to the highly delocalized π-electron system of the guanidinium group, which undergoes strong π→π* and n→π* transitions in the deep UV that tail significantly into the >200 nm region. The carboxylate group ($-COO^-$) also contributes to this absorption. The hydrolysis product, L-ornithine, lacks this conjugated guanidinium system, resulting in a sharp decline in absorbance at wavelengths greater than 195 nm. The wavelength of 200 nm was selected for UV absorption monitoring to provide optimal contrast. The calculated molar extinction coefficients at 200 nm are ~ 2650 M^{-1} cm^{-1} for L-arginine and 750 M^{-1} cm^{-1} for L-ornithine. This difference of more than 3.5-fold makes this wavelength highly sensitive for recording substrate depletion.

The CD spectra (Figure 2a) reflect how these chromophores behave within the chiral environment dictated by the α-carbon. L-arginine (red line) displays a complex profile featuring a sharp local minimum at ~198 nm and a broad, intense positive maximum in the 205–210 nm range. This profile is the result of overlapping π→π* and n→π* transitions of the carboxylate group combined with the intrinsic chiral transitions of the bulky, positively charged guanidinium side chain. When L-arginine is converted to L-ornithine (blue line), the removal of the guanidinium group drastically alters the chiral optical signature. The complex profile disappears, and the spectrum smooths into a single positive band driven by the standard carboxylate transitions. For quantitative kinetic monitoring using CD, 205 nm was selected as the optimal optical window. This specific wavelength offers an excellent signal-to-noise ratio compared to the shorter wavelength region (<200 nm), where intense absorption from the buffer solution and atmospheric oxygen significantly degrades signal quality. Furthermore, 205 nm provides an optimal and easily recordable difference in the CD signal. The L-arginine and L-ornithine molar ellipticities were determined as 2900 deg cm^2 $dmol^{-1}$ and 1700 deg cm^2 $dmol^{-1}$, respectively. Expressed as molar circular dichroism (Δε), this corresponds to 0.88 M^{-1} cm^{-1} for L-arginine versus 0.52 M^{-1} cm^{-1} for L-ornithine. Combined monitoring at 200 nm (UV absorption) and 205 nm (CD) effectively isolates the substrate's structural transformation, providing optimal, interference-free windows for real-time kinetic analysis.

To apply this approach to biomedical formulations, we selected liposomes due to their propensity to target the liver—the primary site of hepatocellular carcinoma and metastases, which are the main clinical indications for arginase therapy. We evaluated free arginase and liposomal arginase, including an enzyme-free negative control to rule out spontaneous hydrolysis. Since the highly scattering, turbid lipid matrix could potentially obscure the far-UV diagnostic spectra, the lipo-ARG formulation was synthesized and characterized to confirm the analytical method's applicability to complex media.

3.3. Preparation and Characterization of Liposomal Formulations

The successful encapsulation of the Mn-activated enzyme into phospholipid vesicles was achieved using a thin-lipid-film hydration method followed by sequential extrusion. The chosen lipid matrix comprised phosphatidylcholine (PC) and cardiolipin (CL) at an 80:20 molar ratio.

The key physicochemical characteristics of the resulting lipo-ARG formulation are summarized in Table 2.

Table 2. Physicochemical characteristics of the liposomal arginase (lipo-ARG) formulation.

Parameter	Value
Lipid composition (mol%)	PC:CL (80:20)
Final lipid-to-protein mass ratio (*w*/*w*)	3:1
Final lipid-to-protein molar ratio	~345:1 (per arginase trimer)
Z-average hydrodynamic diameter (nm)	165 ± 12
Polydispersity index (PDI)	0.14 ± 0.02
Zeta potential (mV)	−35 ± 4
Enzyme encapsulation efficiency (%)	43 ± 5

The inclusion of CL was specifically intended to impart a strong negative surface charge to the resulting vesicles, which is a critical parameter for preventing aggregation and ensuring long-term colloidal stability. Following sequential extrusion through 400 nm and 200 nm polycarbonate membranes, dynamic light scattering analysis confirmed the formation of a highly uniform vesicle population. The liposomes exhibited a Z-average hydrodynamic diameter of 165 ± 12 nm paired with a low polydispersity index of 0.14 ± 0.02. Furthermore, the zeta potential of the lipo-ARG formulation was measured at –35 ± 4 mV. When compared to empty control PC:CL liposomes, which typically exhibit a significantly more negative zeta potential (~–50 mV), this distinct positive shift provides direct evidence of charge compensation. It confirms the active involvement of the anionic cardiolipin headgroups in electrostatically binding the protein and its associated cations. Nevertheless, the remaining net negative charge of –35 mV confirms the anticipated electrostatic stabilization provided by the CL component, remaining well within the required range to prevent vesicle aggregation.

The separation of the unencapsulated arginase via dialysis using a 300 kDa cutoff membrane enabled the accurate quantification of the encapsulation efficiency, which reached 43 ± 5%. Consequently, the final, purified liposome formulation possesses an optimized lipid-to-protein mass ratio of 3:1, corresponding to a molar ratio of approximately 345:1 per arginase trimer. This robust loading capacity is achieved through both aqueous core entrapment and interfacial binding. Specifically, the excess of essential Mn^{2+} ions associated with the enzyme is hypothesized to participate in electrostatic interactions with the anionic cardiolipin domains, contributing to the recruitment and association of arginase with the bilayer surface. This physical encapsulation strategy preserves the natural catalytic conformation of the enzyme while providing necessary steric and electrostatic

shielding, offering a substantial functional advantage over existing covalent PEGylation or metal-substitution techniques.

3.4. Real-Time Kinetic Monitoring of Free and Liposomal Arginase via CD and UV Spectroscopy

Prior to continuous kinetic monitoring, the experimental parameters were specifically optimized to accommodate the distinct physical constraints of transmission-based UV/CD versus surface-based ATR-FTIR spectroscopy. Because mammalian arginases are not subject to substrate inhibition, all assays were intentionally conducted under strict substrate-saturating conditions (≥20 mM, V_{max} regime) to accurately derive catalytic constants. For CD and far-UV absorbance performed in 1-mm transmission cuvettes, 20 mM L-arginine represents the absolute optimal concentration. Exceeding this threshold results in profound deep-UV photometric saturation due to the intense total absorption of the guanidinium groups, drastically reducing the signal-to-noise ratio. Conversely, ATR-FTIR relies on an evanescent wave penetrating only 1–2 micrometers into the sample; therefore, a higher substrate concentration (30 mM) was employed for IR measurements to yield highly resolved, high-contrast vibrational spectra. Furthermore, varying enzyme loading doses were deliberately utilized across the different modalities to confirm dose-dependence, validate the dynamic range of the developed toolkit, and ensure that the derived intrinsic k_{cat} remain robust and independent of absolute enzyme concentration.

To quantitatively evaluate the catalytic performance of both free and encapsulated arginase, the continuous enzymatic hydrolysis of 20 mM L-arginine was monitored in real-time. Figure 3 displays the time-resolved spectral changes recorded over a 20-min reaction period. For both the free (Figure 3a) and liposomal (Figure 3b) enzyme preparations, a progressive, time-dependent decrease in the CD ellipticity was observed. As the reaction proceeded, the characteristic bimodal profile of L-arginine gradually flattened, smoothly transitioning toward the spectral signature of the product, L-ornithine.

Concurrently, the time-dependent UV absorption spectra for both the free (Figure 3c) and liposomal (Figure 3d) arginase exhibited a rapid, steady decay in absorbance, directly reflecting the cleavage of the strongly absorbing guanidinium moiety. Notably, the UV absorption spectra in both cases enter a region of severe detector saturation (photometric overflow) at wavelengths below 195–200 nm. This massive general over-absorption is primarily driven by the extremely high intrinsic absorbance of the concentrated substrate (20 mM L-arginine) combined with the inherent absorption of the aqueous medium in the deep-UV region. This is a fundamental optical limitation of the system as a whole, which is only further compounded by the turbidity of the lipid vesicles in the liposomal sample (Figure 3d). Consequently, the spectral region below 200 nm is analytically unreliable and is intentionally excluded from the quantitative evaluation. The carefully selected diagnostic wavelength of 200 nm is positioned optimally at the edge of this saturation threshold, completely bypassing the deep-UV noise while remaining within the reliable linear dynamic range of the spectrometer. The successful acquisition of these dynamic spectra at 200 nm confirms that the phospholipid bilayer permits unimpeded substrate influx and product efflux while remaining sufficiently optically transparent in the precise diagnostic measurement windows required for accurate kinetic tracking.

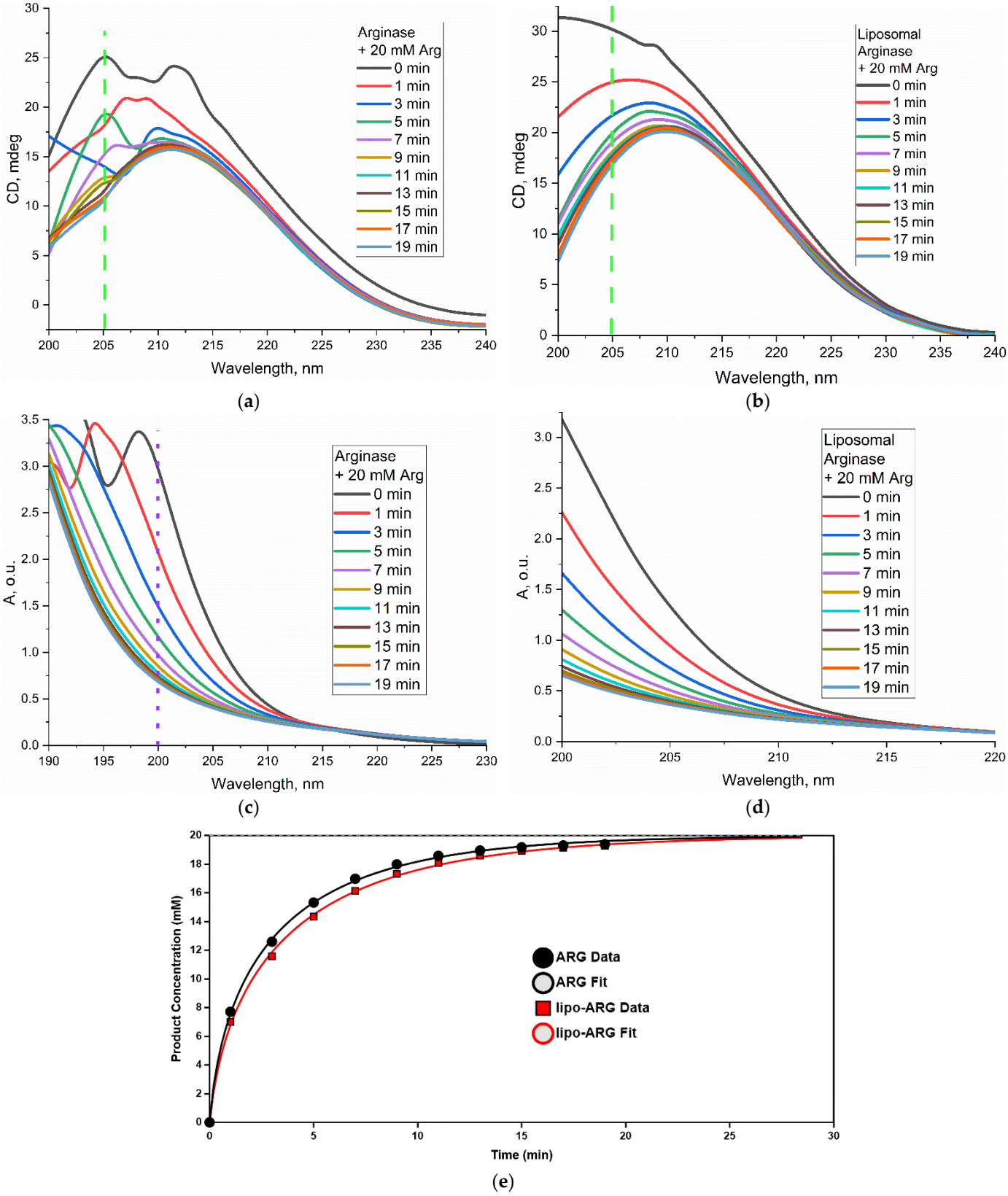


Figure 3. Real-time monitoring of L-arginine hydrolysis by free and liposomal arginase using CD and UV spectroscopy. Time-dependent CD spectra of 20 mM L-arginine incubated with (**a**) free arginase and (**b**) liposomal arginase. Corresponding time-dependent UV absorption spectra for (**c**) free arginase and (**d**) liposomal arginase. Spectra were recorded over a 20-min period. (**e**) Kinetic curves depicting product concentration over time derived from the spectral data for free arginase (black circles) and liposomal arginase (red squares), fitted to a kinetic model.

By converting the time-dependent spectral changes into product concentrations, comparative kinetic progress curves were constructed (Figure 3e). Both enzyme formulations demonstrated a characteristic kinetic profile featuring a rapid initial phase of product accumulation that gradually plateaued as the initial 20 mM substrate was consumed. The trajectory of the progress curve for free arginase (black circles) indicates a marginally steeper initial reaction rate compared to that of the liposomal arginase (red squares). Control experiments performed under identical conditions in the absence of the enzyme exhibited absolutely no spectral changes over the observation period, confirming that no spontaneous hydrolysis of L-arginine occurs and that the recorded signal decay is strictly driven by the enzymatic reaction.

Because the kinetics were evaluated over the full reaction time-course, the depletion of the substrate is accompanied by the substantial accumulation of L-ornithine, a known competitive inhibitor of mammalian arginases. Therefore, the kinetic parameters were derived by non-linear regression using the numerical integration of the differential rate equation that explicitly accounts for competitive product inhibition:

$$d[S]/dt = -V_{max} \times [S]/\{ K_M \times (1 + [P]/K_i) + [S]\}$$

where $[P] = [S]_0 - [S]$, and K_i is the inhibition constant for L-ornithine. The fitting model successfully resolved the inhibition constants for both formulations directly from the full progress curves. It is extensively documented in the biochemical literature that L-ornithine acts as a strong competitive inhibitor of mammalian arginases [30]. While an independent multi-concentration inhibition assay is required to define an absolute, definitive inhibition constant, our primary objective herein was to mathematically describe the full continuous progress curve of the spectroscopic assay. During data modeling, fitting the experimental data to a simple integrated Michaelis–Menten equation lacking an inhibition term resulted in poor fits with severe systematic deviations in the later stages of the substrate depletion trajectory. Conversely, incorporating the competitive product inhibition term into the differential rate equation yielded an excellent fit ($R^2 > 0.99$) for the entire reaction course. Therefore, the K_i values reported in this model are derived primarily from the shape of the progress curve to mathematically constrain the later stages of the reaction. They should be interpreted as apparent operational constants that ensure the highly accurate extraction of V_{max} and K_M. Crucially, the resulting apparent Ki values obtained for both native arginase (3.55 ± 0.30 mM) and liposomal arginase (5.20 ± 0.45 mM) summarized in Table 3 fall squarely within the established literature range, confirming the physical and mathematical validity of the applied kinetic model.

For the free enzyme, the inhibition constant is comparable to the Michaelis constant (K_i = 3.55 ± 0.30 mM), which significantly modulates the curvature of the progress curve in its later stages. Interestingly, for the liposomal formulation, the K_i value notably increased to 5.20 ± 0.45 mM. This apparent reduction in product inhibition suggests that the phospholipid bilayer microenvironment either facilitates the rapid outward diffusion of L-ornithine or sterically limits its rebinding at the compartmentalized active site. The resulting statistical errors for the extracted parameters were thoroughly analyzed to confirm the robustness of this kinetic model.

The quantitative kinetic parameters extracted from these models are summarized in Table 3. The native, free arginase exhibited a maximum reaction velocity (V_{max}) of 9.45 ± 0.42 mM/min and a turnover number k_{cat} of 276 s^{-1}. Liposomal arginase, showed a minor reduction in V_{max} to 8.57 mM/min, corresponding to a k_{cat} of 250 s^{-1}. The standard deviations for V_{max} and k_{cat} are relatively small (approximately 4–5%), indicating a high precision of the fitting model across the entire progress curve. Importantly, the statistical errors for the liposomal formulation (e.g., ±0.38 mM/min for V_{max}) are comparable to those of the free enzyme (±0.42 mM/min). This confirms that the highly scattering liposomal matrix

does not introduce significant optical noise or systemic artifacts into the calculated parameters. Notably, the Michaelis constant K_M remained essentially unchanged between the free (3.60 ± 0.25 mM) and liposomal (3.65 ± 0.27 mM) formulations. As a result, the overall catalytic efficiency k_{cat}/K_M of the liposomal arginase was determined to be (6.8 ± 0.5) × 10^4 $s^{-1}M^{-1}$, demonstrating that the encapsulated enzyme retains approximately 90% of the native catalytic efficiency observed for the free enzyme (7.6 ± 0.6) × 10^4 $s^{-1}M^{-1}$. The concurrent increase in the Ki value for the liposomal form provides an additional functional advantage by delaying the onset of product inhibition during continuous catalytic turnover in confined environments.

Table 3. Kinetic parameters of arginase activity obtained by CD spectroscopy. Data are presented as mean ± SD. The kinetic parameters were calculated using non-linear least-squares fitting of the full product accumulation curves to the differential rate equation incorporating competitive product inhibition. The initial substrate concentration was $[S]_0$ = 20 mM, and the enzyme concentration was $[E]_0$ = 0.02 mg/mL. The catalytic constant was calculated assuming a monomer molecular weight of ~35 kDa for arginase.

Parameter	Native Arginase	Liposomal Arginase *
V_{max}, mM/min	9.45 ± 0.42	8.57 ± 0.38
K_M, mM	3.60 ± 0.25	3.65 ± 0.27
K_i, mM	3.55 ± 0.30	5.20 ± 0.45
k_{cat}, s^{-1}	276 ± 12	250 ± 11
k_{cat}/K_M, $s^{-1}\times M^{-1}$	(7.6 ± 0.6) × 10^4	(6.8 ± 0.5) × 10^4

* The enzyme concentration [E]0 used to calculate k_{cat} refers to the actual encapsulated protein concentration present in the purified vesicles, determined via post-dialysis quantification.

To validate the accuracy of the proposed reagent-free continuous CD assay, these kinetic parameters for the native bovine arginase were compared with standard literature values acquired using traditional end-point colorimetric methods, such as the diacetyl monoxime assay utilized for urea quantification. The calculated K_M value of 3.60 mM and the k_{cat} of 276 s^{-1} are in excellent agreement with previously reported kinetic constants for bovine liver arginase (arginase I) [3], which typically displays a K_M ranging from 2.0 to 4.5 mM and a turnover number between 200 and 350 s^{-1} depending on the specific experimental buffer and temperature conditions. Furthermore, these values align closely with the catalytic profiles of other well-characterized mammalian arginases, such as human arginase I, for which literature sources generally report a comparable K_M of approximately 2.0 to 4.0 mM. The strong correlation between the CD-derived kinetic parameters and the established colorimetric literature data for these homologous enzymes confirms that the direct spectroscopic monitoring of the L-arginine to L-ornithine conversion provides a highly accurate and reliable measurement of continuous enzymatic activity without the need for auxiliary reagents or structural derivatization.

3.5. ATR-FTIR Spectroscopic Monitoring of Substrate Depletion and Product Formation

To complement the far-UV CD measurements, attenuated total reflectance Fourier-transform infrared (ATR-FTIR) spectroscopy was developed as an orthogonal analytical method to monitor the enzymatic reaction. This approach is fundamentally based on tracking the dynamic changes in specific vibrational peak intensities that directly correspond to the depletion of the L-arginine substrate and the concomitant accumulation of the L-ornithine product over the course of the hydrolysis process. Figure 4a presents the reference ATR-FTIR spectra of 30 mM L-arginine and 30 mM L-ornithine, with the comprehensive vibrational band assignments detailed in Table 4.

Table 4. FTIR band assignment of L-arginine (substrate) and L-ornithine (product), 850–1750 cm^{-1}.

Wavenumber, cm^{-1}	Vibrational Mode	L-Arginine	L-Ornithine	Diagnostic Use in Kinetic Monitoring
~1675	ν_{as} $CN_3H_5^+$ (guanidinium, high-frequency component)	Strong	Absent	Substrate-specific; decay tracks arginine consumption
~1630	ν_{as} $CN_3H_5^+$ (guanidinium, low-frequency component); overlapping ν_{as} COO^- (Arg)	Strong (doublet component + carboxylate overlap)	Absent (guanidinium); weak (carboxylate only)	Substrate-specific; the 1630/1675 cm^{-1} doublet is the primary kinetic marker for L-Arg
~1605	ν_{as} COO^- (carboxylate)	Weak/overlapping	Strong	Product-specific; rises as ornithine accumulates
~1520	δ_s NH_3^+ (ammonium bending)	Absent	Strong	Product-specific; confirms the α-amino/δ-amino ammonium environment unique to ornithine
~1410	ν_s COO^- (carboxylate, symmetric)	Weak	Strong	Product-specific; complements the 1605 cm^{-1} band for ornithine quantification
~1355	ω CH_2 (methylene wagging)	Weak	Strong	Product-specific; reports on the shorter, more flexible ornithine side chain
1050–980	ν C–N/C–C (aliphatic backbone/side-chain stretch)	Present (unique envelope)	Negligible	Substrate-specific secondary marker, confirms the guanidinium-doublet assignment

The infrared spectrum of L-arginine is strongly characterized by the asymmetric stretching modes of the guanidinium group (ν_{as} $CN_3H_5^+$), which appear as a prominent high-frequency component at ~1675 cm^{-1} and a low-frequency component at ~1630 cm^{-1}. An additional unique envelope is present at 1050–980 cm^{-1}, corresponding to aliphatic backbone and side-chain stretches. Conversely, the spectrum of the product, L-ornithine, lacks these guanidinium signatures entirely. Instead, it is dominated by strong product-specific bands, most notably the carboxylate asymmetric stretch (ν_{as} COO^-) at ~1605 cm^{-1}, the ammonium bending mode (δ_s NH_3^+) at ~1520 cm^{-1}, and the symmetric carboxylate stretch (ν_s COO^-) at ~1410 cm^{-1}. The distinct separation between the substrate-specific ~1675 cm^{-1} band and the product-specific ~1520 cm^{-1} band provides an optimal, interference-free system for quantitative kinetic tracking.

The real-time catalytic conversion of 20 mM L-arginine was continuously monitored by recording sequential FTIR spectra. For the reaction catalyzed by free arginase (Figure 4b), the time-resolved spectra over 13 min revealed a systematic, progressive depletion of the substrate-specific guanidinium bands, accompanied by the proportional emergence of the ornithine-specific bands. An identical spectral evolution was successfully recorded for the liposomal arginase formulation over 9 min (Figure 4c). The clear detection of these vibrational transitions in the encapsulated sample confirms that the presence of the phospholipid bilayer does not obscure the diagnostic infrared windows, thereby allowing direct tracking of intra-liposomal substrate processing. By integrating the changes in the diagnostic absorption bands, kinetic progress curves detailing product accumulation over time were constructed (Figure 4d).

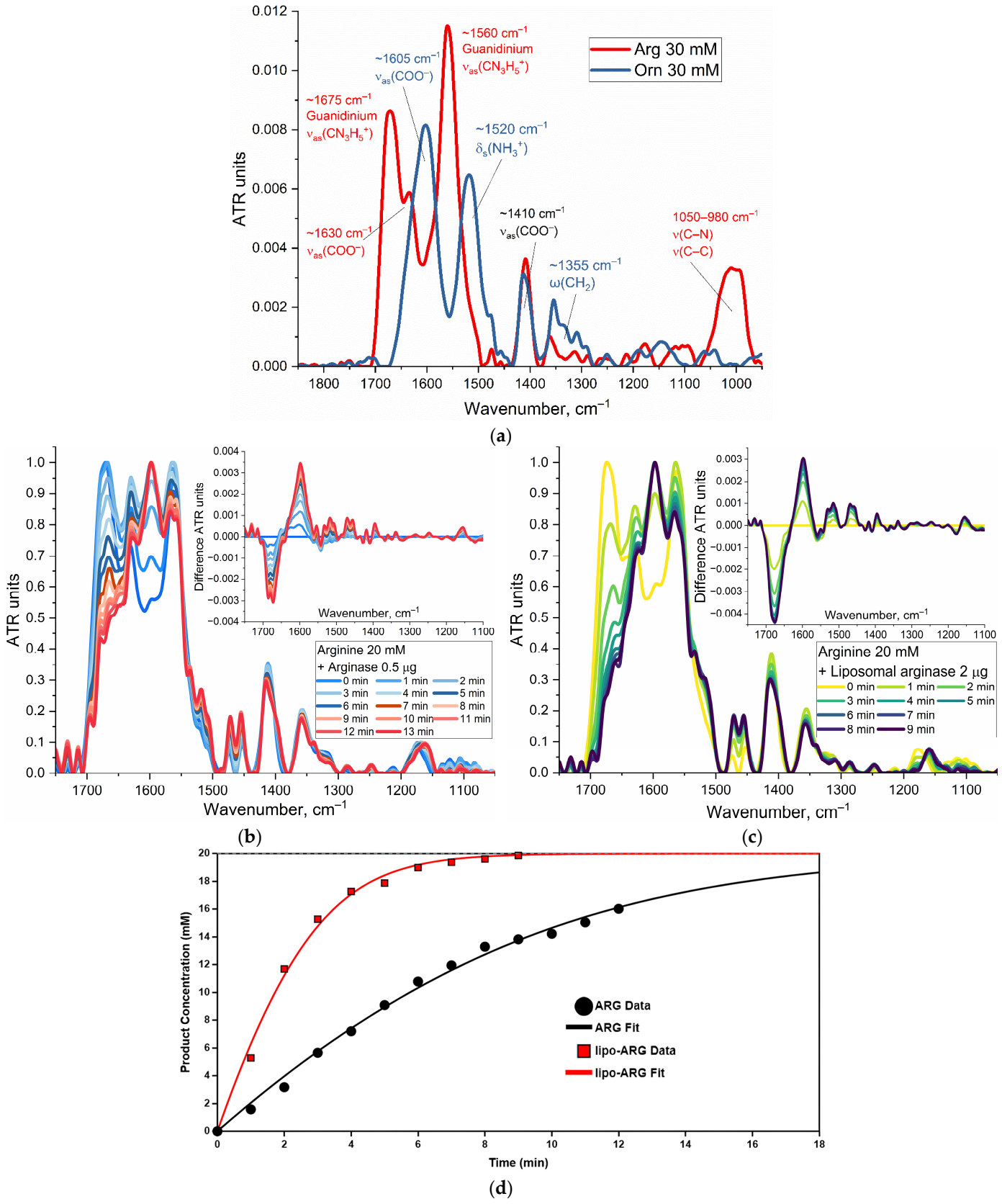


Figure 4. ATR-FTIR spectroscopic analysis of arginase catalytic kinetics. (**a**) Reference ATR-FTIR spectra of 30 mM L-arginine (red line) and 30 mM L-ornithine (blue line) displaying major vibrational band assignments, accompanied by the chemical structures of the substrate and product to illustrate the cleaved guanidinium moiety. Time-resolved ATR-FTIR spectra tracking the hydrolysis of 20 mM L-arginine catalyzed by (**b**) 0.5 μg of free arginase and (**c**) 2 μg of liposomal arginase as representative examples. Difference spectra demonstrating the increase in the product band and

decrease in the substrate band is shown in insert (**b,c**). Arrows indicate the direction of spectral changes over time: the downward decay of the substrate bands (1675 cm^{-1}) and the upward emergence of the product band (~1605 cm^{-1}). (**d**) Kinetic curves (by 1690 cm^{-1} band) of product accumulation over time derived from the FTIR spectra for free arginase (black circles) and liposomal arginase (red squares). The differing curve trajectories directly reflect the deliberate application of different enzyme doses (0.5 µg versus 2 µg) in order to test and validate the dynamic range and versatility of the developed spectroscopic method.

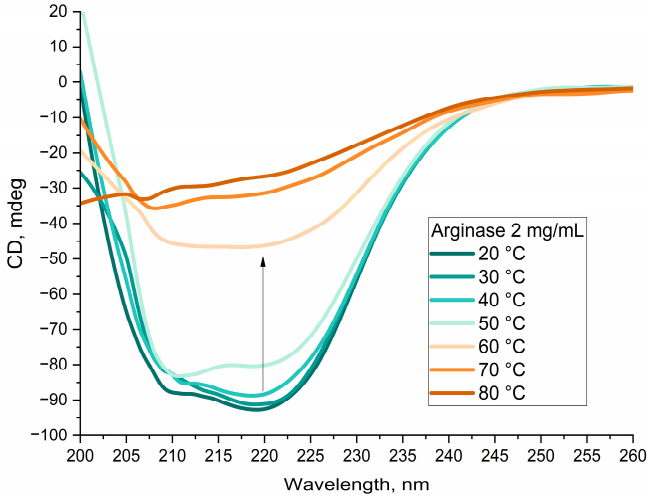
The kinetic parameters derived from FTIR data are summarized in Table 5. Native free arginase exhibited K_M of 1.34 ± 0.10 mM, and a turnover number of 314 ± 16 s^{-1}, yielding a catalytic efficiency of (2.3 ± 0.2) × 10^5 $s^{-1}M^{-1}$. Upon liposomal encapsulation, the apparent K_M slightly increased to 2.08 mM, and the turnover number experienced a minor reduction to 285 ± 14 s^{-1}. Consequently, catalytic efficiency of the liposomal arginase was determined to be 1.37 × 10^5 $s^{-1}M^{-1}$. FTIR-derived parameters corroborate the findings of the CD assay, confirming that the enzyme retains a high degree of its native catalytic capacity following incorporation into the lipid vesicles.

Table 5. Kinetic parameters of arginine hydrolysis determined using ATR-FTIR spectroscopy. Data are presented as mean ± SD. The parameters were mathematically extracted by fitting the numerical integration of the differential rate equation (incorporating product inhibition) to the full, continuous product-accumulation curves. To ensure maximum spectral signal-to-noise ratio for parameter estimation, the initial substrate concentration for these specific fitting datasets was set to $[S]_0$ = 30 mM. The active enzyme concentrations in the reactor were $[E]_0$ = 0.004 mg/mL for free arginase and 0.015 mg/mL for liposomal arginase (reflecting exclusively the encapsulated protein fraction). The k_{cat} is strictly normalized to these respective $[E]_0$ values, calculated assuming a monomer molecular weight of ~35 kDa for arginase.

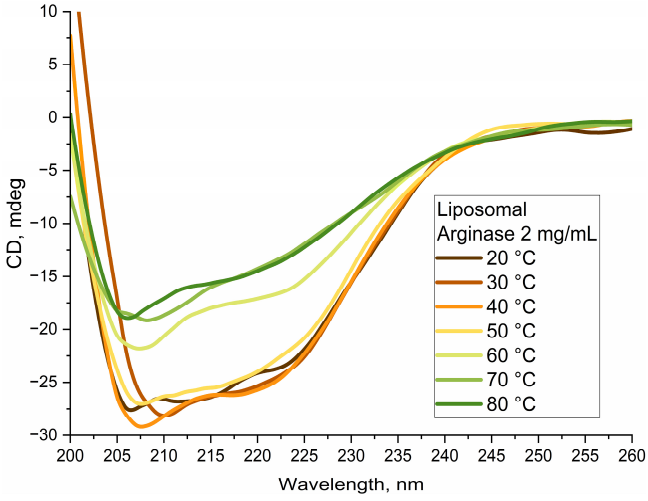
Parameter	Native Arginase	Liposomal Arginase
K_M, mM	1.34 ± 0.10	2.08 ± 0.15
k_{cat}, s^{-1}	314 ± 16	285 ± 14
k_{cat}/K_M, $s^{-1}\times M^{-1}$	(2.3 ± 0.2) × 10^5	(1.37 ± 0.11) × 10^5

3.6. Influence of Liposome Encapsulation on the Conformational Properties and Stability of Arginase

To determine whether the phospholipid bilayer alters the conformational stability of the enzyme, the thermal denaturation of free and liposomal arginase (2 mg/mL) was monitored from 20 to 80 °C by far-UV CD and UV absorption spectroscopy (Figure 5).



(**a**)



(**b**)

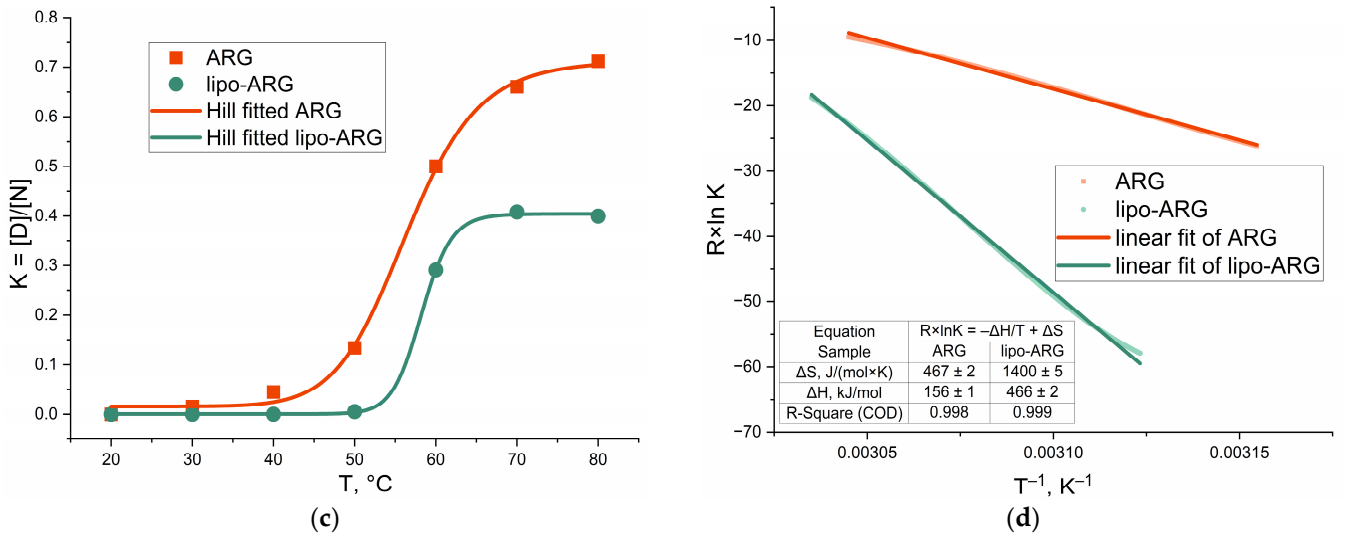


Figure 5. Thermal stability and thermodynamic analysis of free and liposomal arginase. Temperature-dependent CD spectra (20–80 °C) of (**a**) free arginase and (**b**) liposomal arginase (2 mg/mL). (**c**) Fraction of unfolded protein (equilibrium constant K) versus temperature for free (ARG) and liposomal (lipo-ARG) arginase. (**d**) Van't Hoff plot (R·ln K vs. T^{-1}) used to obtain the enthalpy (ΔH) and entropy (ΔS) of unfolding.

To quantitatively determine the influence of liposomes on the secondary structure and its resistance to thermal denaturation, a CDNN deconvolution of the CD spectra was performed (Figure 6). Although the raw spectra exhibit apparent visual differences due to the intense optical scattering of the lipid vesicles, the CDNN algorithm effectively normalizes these amplitude variations. The deconvolution analysis reveals that at baseline temperatures (20–50 °C), the secondary-structure composition of lipo-ARG (α-helix ~18–20%, β-sheet ~24–25%, β-turn ~18%, random coil ~38–39%) is structurally highly consistent with that of the free enzyme (α-helix ~16–17%, β-sheet ~26%, β-turn ~18%, random coil ~40%). Therefore, the liposomal formulation successfully preserves the native structural fold upon encapsulation.

Above 50 °C, the thermal denaturation trajectories of the two formulations diverge significantly. Free arginase experiences severe structural degradation, losing approximately one-third of its helical content (dropping from ~16% at 50 °C to ~11% at 80 °C). This lost helical structure is primarily redistributed into β-sheets, which increase from ~26% to ~30%. This structural transition is consistent with the collapse of the characteristic 208/222 nm double minimum into a single broad minimum near 215 nm in the raw spectra, providing a clear spectroscopic marker for progressive intermolecular β-aggregation.

In contrast, the liposomal formulation exhibits profoundly enhanced structural stability under identical thermal stress. For lipo-ARG, the α-helical content is strongly conserved, decreasing only from ~18.5% at 50 °C to ~14.5% at 80 °C, while the β-sheet fraction experiences a vastly suppressed expansion, shifting only from ~25% to ~27%. These quantitative findings confirm that anchoring the enzyme within the phospholipid bilayer severely restricts large-scale unfolding and almost entirely prevents heat-induced β-aggregation, rendering the liposomal formulation significantly more stable than the native enzyme under acute thermal stress.

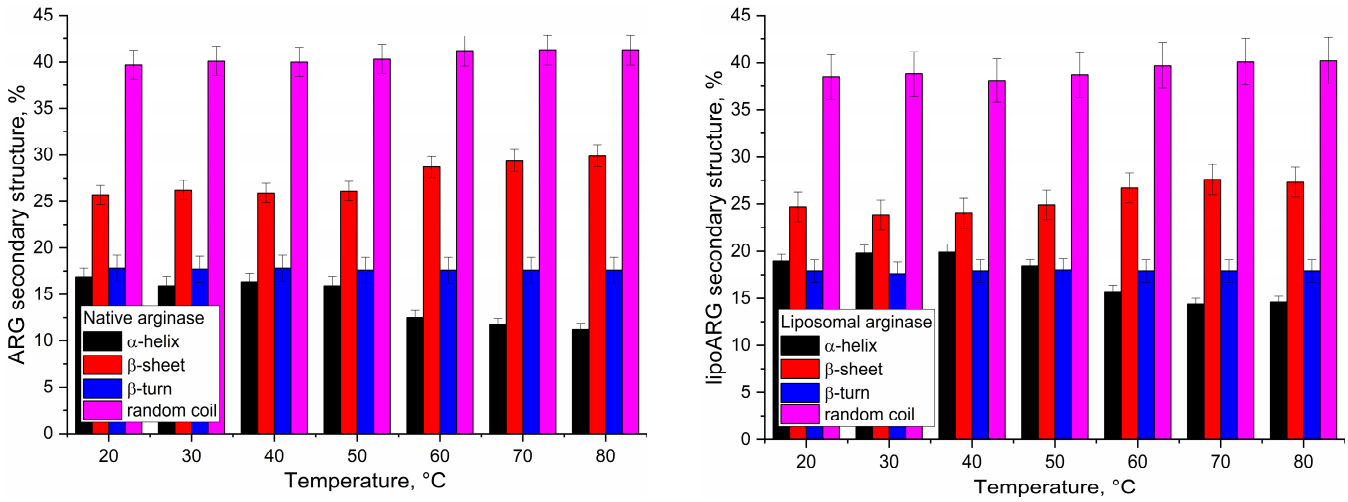


Figure 6. CDNN-deconvoluted secondary-structure composition (α-helix, β-sheet, β-turn, random coil; normalized to 100%) of (**a**) free arginase and (**b**) liposomal arginase as a function of temperature 20–80 °C.

Having established that the liposomal bilayer successfully preserves the secondary structure of arginase, we next sought to evaluate whether this protective effect extends to the tertiary packing and the local environment of aromatic residues. To achieve this, we employed second-derivative UV absorption spectroscopy, which provides an independent, scattering-free readout of the tryptophan (Trp, ~291 nm) and tyrosine (Tyr, ~283 nm) signals (Figure 7a,b).

Focusing first on the hydrophobic core, we observed that across the 20–80 °C heating range, the position of the Trp second-derivative peak remained invariant (290.9 ± 0.1 nm) for both formulations (Figure 7d). Thermal unfolding does not fully expose the internal indole rings to the bulk solvent. However, the peak amplitude as a sensitive reporter of local structural perturbation, increased by ~30% for the free arginase upon heating (Figure 7c), consistent with a progressive loosening of the tertiary packing. In contrast, the encapsulated arginase exhibited a ~45% higher baseline amplitude at 20 °C (0.0024 a.u.), implying that the membrane anchoring itself intrinsically perturbs the resting Trp environment. More importantly, this amplitude increased by only 10–15% upon subsequent heating (Figure 7c), confirming that liposomal encapsulation severely dampens the thermal response of the protein core without altering its overall fold class.

While the Trp signal primarily reflects the stabilization of the internal protein core, monitoring the tyrosine (Tyr) signature provided critical insights into the external protein-lipid interface. Specifically, in the liposomal formulation, the Tyr peak position exhibited a distinct, progressive wavelength shift (from ~282.6 to ~284.8 nm) that synchronized precisely with the thermal melting of the lipid bilayer (Figure 7f). This targeted spectral shift is consistent with tyrosine residues experiencing altered local microenvironments at the protein–lipid interface, suggesting protein–lipid interactions that accompany stabilization. In stark contrast, the Tyr peak position of the free native enzyme remained relatively static (~284.0 nm) across the same temperature range (Figure 7f). Devoid of this stabilizing lipid interface, the free native enzyme simply undergoes global structural collapse, leading to the aggregation previously observed in CD spectra.

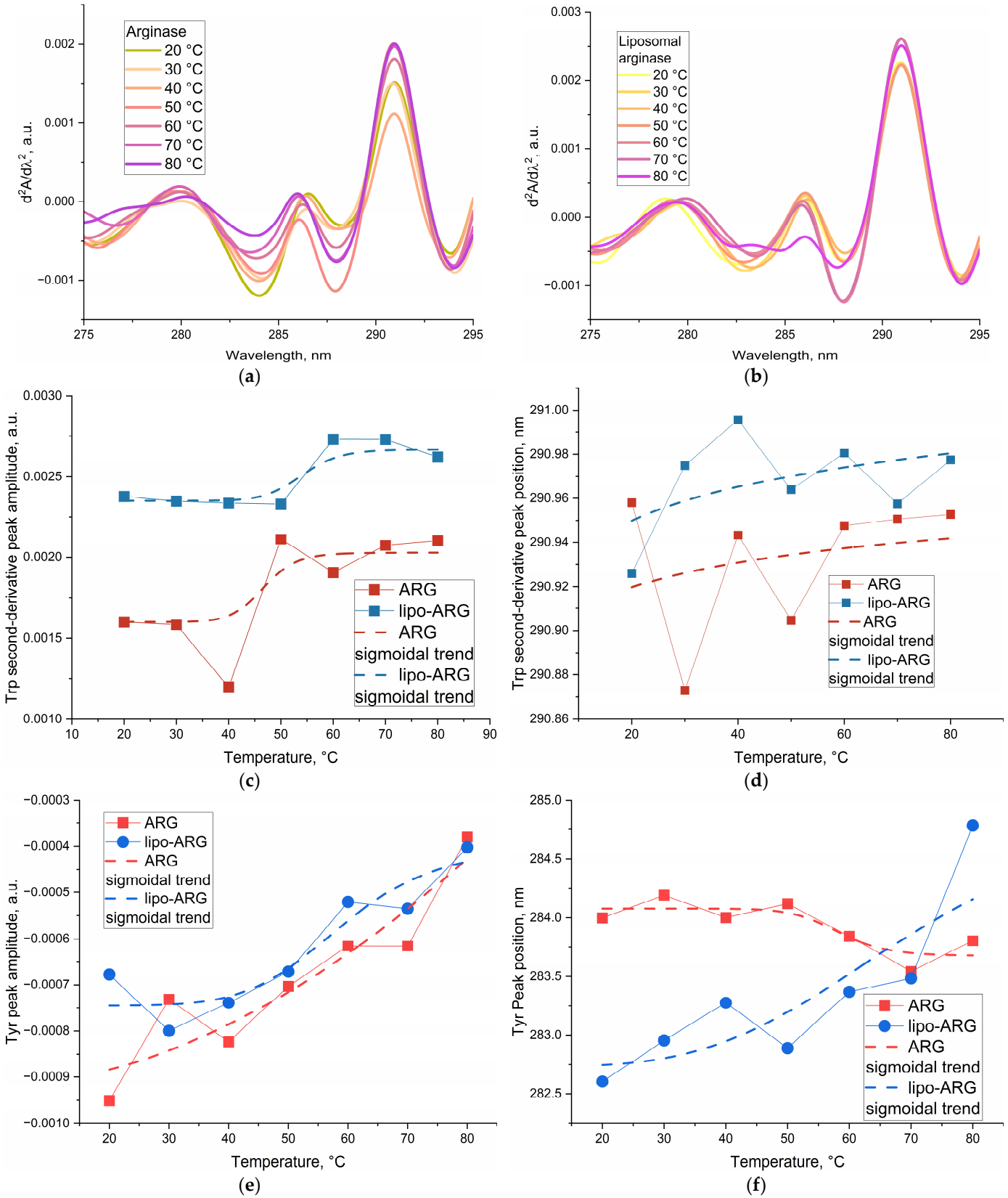


Figure 7. Second-derivative UV absorption analysis of the Trp/Tyr region (250–300 nm) of free (ARG) and liposomal (lipo-ARG) arginase at 20–80 °C. Second-derivative spectra of (**a**) ARG and (**b**) lipo-ARG at all seven temperatures. (**c**) Amplitude and (**d**) position of the Trp second-derivative peak (≈291 nm) versus temperature. (**e**) Amplitude and (**f**) position of the Tyr second-derivative peak (≈283 nm) versus temperature.

So, scattering-free readouts perfectly complement the CDNN analysis, confirming a dual mechanism of liposomal protection: the preservation of the secondary fold and the locking of the tertiary core via direct membrane anchoring. Since we have now biophysically established that the lipid matrix effectively prevents heat-induced structural aggregation, the logical next step is to evaluate how this macromolecular lockdown translates into functional resilience. To this end, we subsequently investigated the kinetics of thermal inactivation to quantify the preservation of residual catalytic activity.

3.7. Kinetics of Irreversible Thermal Inactivation and Functional Stabilization of Liposomal Arginase

Given the thermodynamic restriction of global unfolding established above, we next asked how it translates into resistance to irreversible thermal inactivation. Free and liposomal arginase were incubated at 55 °C and 70 °C, cooled, and residual activity (A/A_0) was measured by the CD assay at a saturating substrate concentration (15 mM, zero-order conditions; Figure 8).

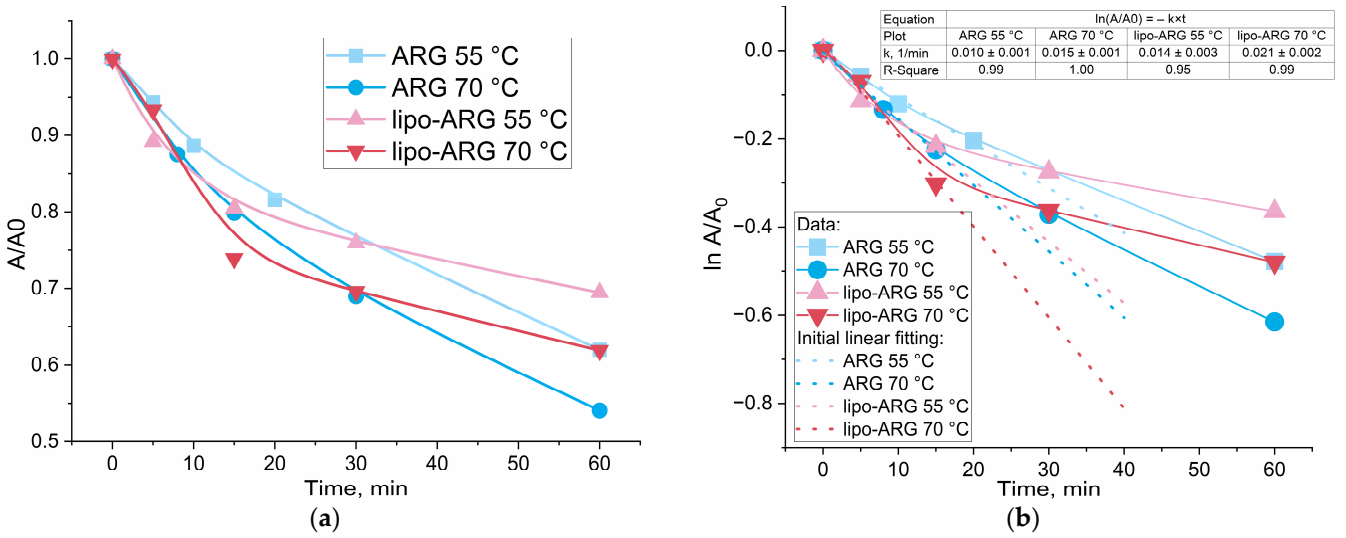


Figure 8. Kinetics of irreversible thermal inactivation of arginase. (**a**) Residual activity (A/A_0) versus incubation time for free and liposomal arginase at 55 °C and 70 °C, measured after cooling. (**b**) Semi-logarithmic plot $\ln(A/A_0)$ vs. time; increasing values correspond to decreasing activity) resolving the biphasic inactivation of lipo-ARG. Dashed lines are linear fits to the initial phase (0–15 min) used to extract k_{in}.

Here, an important methodological distinction between reversible equilibrium thermodynamics and irreversible kinetic processes must be discussed. In applied protein biophysics, the thermal denaturation of complex oligomeric enzymes is often accompanied by irreversible intermolecular aggregation at elevated temperatures, which precludes a true reversible two-state equilibrium. Nevertheless, applying the standard van't Hoff formalism to circular dichroism melting thermograms remains the most widely accepted and indispensable operational approach in the literature for extracting apparent thermodynamic descriptors (apparent ΔH and ΔS). These apparent parameters provide a standardized quantitative metric that is necessary for comparing the relative conformational stability of a native enzyme against its modified counterparts.

To directly address the irreversible component of thermal degradation and determine how the observed structural protection translates into sustained catalytic resilience, the kinetics of irreversible thermal inactivation were independently evaluated. Free and liposomal arginase formulations were incubated at 55 °C and 70 °C, cooled to room temperature, and their residual catalytic activity (A/A_0) was measured via the continuous CD

assay under substrate-saturating conditions (15 mM L-arginine, zero-order regime; Figure 8). In semi-logarithmic coordinates, the resulting inactivation trajectories reveal fundamentally different degradation pathways for the two formulations.

Free arginase exhibits a predominantly first-order exponential decay during the initial heating phase, but noticeably deviates from strict linearity by approximately 15% in the later stages of the incubation. This kinetic deviation directly corroborates our CD spectroscopy and CDNN deconvolution findings, which identified a concurrent 15% shift toward intermolecular antiparallel beta-sheet structures. Because thermal aggregation is a concentration-dependent intermolecular process, it inherently distorts the strictly unimolecular kinetics of simple unfolding, progressively accelerating the loss of activity and pulling the terminal residual activity down to 54% (at 70 °C for 60 min).

Conversely, the liposomal formulation demonstrates a pronounced biphasic inactivation profile, suggesting a heterogeneous thermal response that reflects distinct population states, such as a more labile surface-associated fraction versus a more stable, membrane-protected fraction. During the first 15 min, lipo-ARG inactivates similarly, and even marginally faster, than the free enzyme (k_{in} = 0.014 vs. 0.010 min^{-1} at 55 °C; Table 6). This initial rapid phase is attributed to a minor, loosely associated external fraction residing at the lipid–water interface, which remains exposed to the bulk solvent and acute thermal stress without the full stabilizing benefit of tight membrane association.

Beyond 15 min, however, the liposomal inactivation curve deviates sharply from the initial linear trend and rapidly approaches a stable horizontal plateau. Once the loosely associated fraction is thermally depleted, the more stable, membrane-protected fraction dominates the catalytic response. Shielded from intermolecular collisions and subsequent beta-sheet aggregation through physical association with the cardiolipin-enriched bilayer, this stabilized enzyme population remains robustly active for the remainder of the incubation. Consequently, the liposomal formulation achieves significantly higher terminal residual activity (70% vs. 62% at 55 °C), strongly indicating that macromolecular confinement within the liposomal nanostructure effectively suppresses the irreversible aggregation pathway.

Table 6. Summary of apparent thermodynamic and kinetic parameters of thermal unfolding and inactivation for free and liposomal arginase.

Parameter	Free ARG	Lipo-ARG
$\Delta_{,unf}H_{app}$, kJ/mol	156	466
$\Delta_{,unf}S_{app}$, J/(mol·K)	467	1400
$K_{app,unf}$, unfolding at 80 °C	0.7	0.4
k_{in}, 55 °C, initial phase (min^{-1})	0.010 ± 0.001	0.014 ± 0.003
k_{in}, 70 °C, initial phase (min^{-1})	0.015 ± 0.001	0.021 ± 0.002
E_a, inactivation, initial phase (kJ/mol)	25	25
Residual activity, 55 °C/60 min (%)	62	70
Residual activity, 70 °C/60 min (%)	54	62

3.8. Activation Energy and Mechanistic Pathways of Thermal Inactivation

The activation energy of inactivation, E_a, was obtained from the initial-phase rate constants at 328.15 K and 343.15 K (Arrhenius relationship; Figure 8b). The rate-constant ratio between the two temperatures is identical for free arginase (0.015/0.010) and for the initial phase of lipo-ARG (0.021/0.014), giving the same $E_a \approx 25.3$ kJ/mol for both.

This value is far below the ΔH of global unfolding (156–466 kJ/mol, Section 3.6), showing that the rate-limiting step for early activity loss is not macroscopic unfolding but

a localized event—most likely a conformational fluctuation at the binuclear Mn^{2+} active site or disruption of a peripheral hydrogen-bond network.

The identical E_a for free arginase and the initial phase of lipo-ARG confirms that this vulnerable subpopulation is surface-adsorbed or loosely bound enzyme experiencing an environment equivalent to bulk solvent, rather than the membrane-embedded core.

Once this fraction is depleted, the mechanisms diverge. Free arginase continues to inactivate via irreversible aggregation, consistent with the shift toward intermolecular β-sheet content observed by CD and CDNN deconvolution at high temperature (Figure 6a, Section 3.6). Physical isolation of enzymes within separate liposomes abolishes the intermolecular collisions required for this pathway.

Multipoint anchoring to the bilayer also imposes steric constraints on the deeply embedded core, driving its apparent inactivation rate toward zero: the dominant mechanism shifts from an aggregation-driven cascade to conformational locking, securing the long-term catalytic viability of the formulation.

3.9. Cellular Association and Catalytic Activity of LLC1-Bound Arginase Formulations

Beyond fundamental kinetic validation in model buffer systems, an important objective of this work was to demonstrate the practical applicability of the developed reagent-free spectroscopic platform for quantifying enzymatic activity in optically opaque biological media. Monitoring the real-time catalytic efficiency of therapeutic enzymes in cellular environments is a critical prerequisite for preclinical biomedical applications. To experimentally validate both the analytical performance of the assay in turbid media the enzyme activity was assessed in the presence of cells, murine Lewis lung carcinoma (LLC1) as a relevant oncological model. In the context of targeted cancer therapy, many solid lung tumors exhibit profound arginine auxotrophy due to the metabolic silencing of argininosuccinate synthetase (ASS1), rendering them critically dependent on the uptake of extracellular arginine for survival and proliferation. Consequently, engineering nanocarriers capable of efficiently anchoring highly active arginase directly to the tumor cell surface is a promising strategy to induce localized metabolic starvation, improve local pharmacokinetic profiles, and maximize selective cytotoxic action while minimizing systemic toxicity.

The proposed ATR-FTIR method demonstrates exceptional analytical applicability because measurements in the mid-IR spectral range are fundamentally immune to turbidity and macroscopic light scattering. This unique physical property enables the direct, continuous, and label-free extraction of high-resolution kinetic data from complex biological systems without requiring prior cell lysis, sample purification, or the addition of coupled reporter reagents.

Here, following a 6-h incubation and centrifugal washing to eliminate unbound protein, the cell suspensions were directly analyzed. Figure 9 illustrates the time-resolved ATR-FTIR spectra tracking the continuous hydrolysis of L-arginine catalyzed by the LLC1-bound fractions of arginase (Figure 9a) and liposomal arginase (Figure 9b). The corresponding kinetic trajectories of product accumulation (Figure 9c) reveal a striking functional disparity between the two formulations.

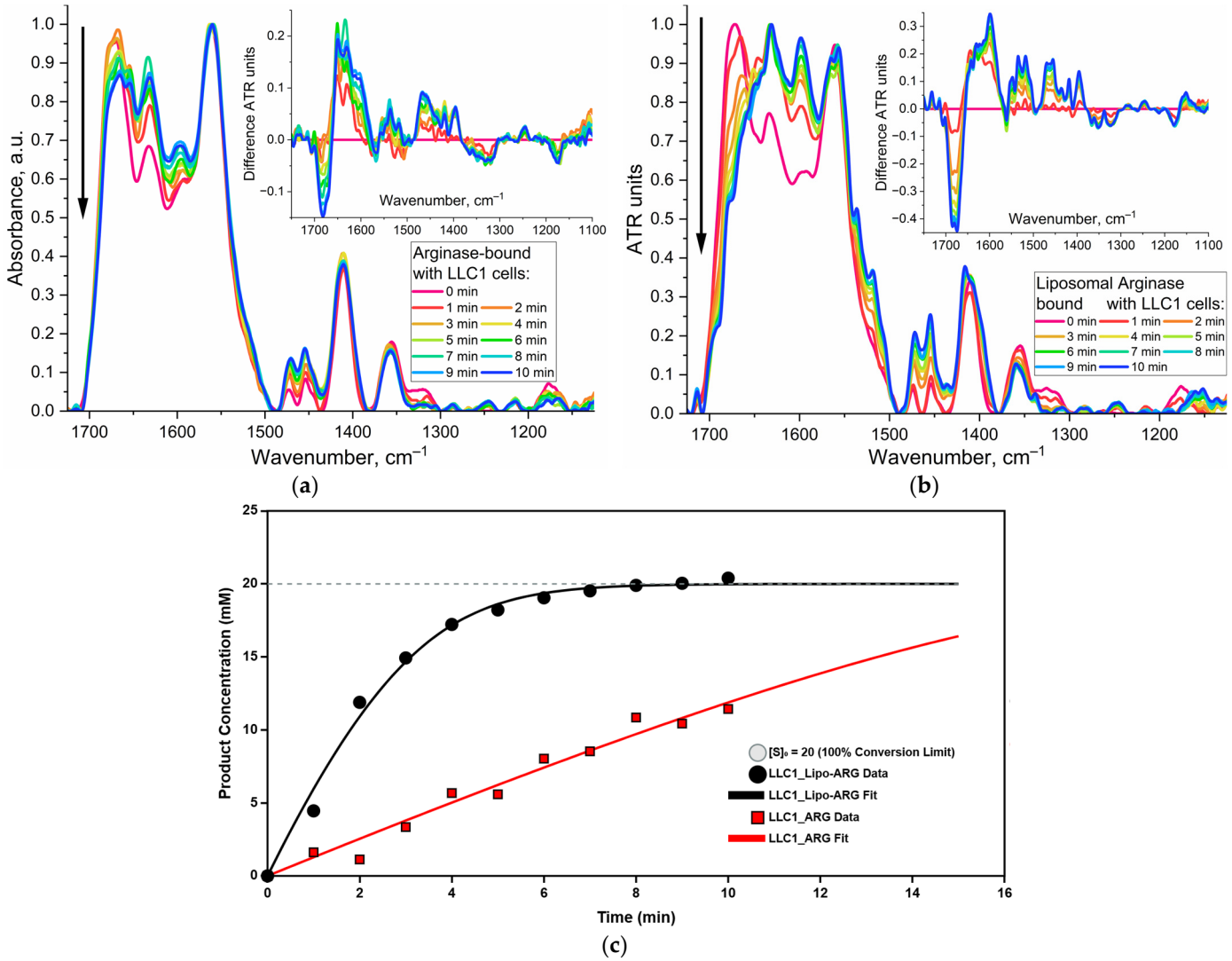


Figure 9. ATR-FTIR spectroscopic evaluation of arginase activity associated with Lewis lung carcinoma (LLC1) cells following a 6-hour incubation period. Time-resolved ATR-FTIR spectra tracking the hydrolysis of L-arginine catalyzed by the washed cell fractions previously treated with (**a**) free arginase and (**b**) liposomal arginase. The downward arrows indicate the time-dependent decay of the substrate-specific guanidinium bands over a 10-minute reaction course. Difference spectra demonstrating the increase in the product band and decrease in the substrate band is shown in insert (**a**,**b**). (**c**) Kinetic progress curves of L-ornithine product accumulation over time derived from the continuous FTIR spectra for the LLC1-bound free arginase (red squares) and LLC1-bound liposomal arginase (black circles). The solid lines represent the corresponding non-linear mathematical fits utilized to extract the initial reaction velocities of the cell-associated enzyme fractions.

We observed that the specific activity of cell-associated liposomal arginase was more than 6.4-fold higher than that of the unencapsulated enzyme (57.5 IU/mg vs. 9.0 IU/mg), normalizing these kinetic rates to the actual amount of cell-bound protein uncovered a critical, previously invisible phenomenon: the severe vulnerability of the naked enzyme to the cellular interface. Upon direct contact with the LLC1 cell surface and pericellular microenvironment, native arginase suffered a dramatic loss of catalytic function, retaining only ~27% of its intrinsic turnover rate (k_{cat} plummeted from 276 ± 12 s^{-1} in PBS buffer to 75.0 ± 6.7 s^{-1} on cells, corresponding to a normalized specific activity of 128.6 ± 11.4 IU/mg). This inactivation likely stems from unfavorable electrostatic or hydrophobic interactions with plasma membrane, surface-induced partial unfolding, or localized proteolytic degradation. In contrast, the liposomal architecture acted as a functional "molecular shield":

cell-bound liposomal arginase preserved ~89% of its native turnover number (k_{cat} = 223.6 ± 4.7 s^{-1}; specific activity of 383.3 ± 8.0 IU/mg per bound protein).

Furthermore, in situ FTIR spectroscopy allowed to quantify the microenvironmental mass-transfer resistance experienced by the enzyme upon cellular immobilization. Both native and liposomal arginase exhibited a ~2-fold increase in apparent K_M on LLC1 cells, reflecting diffusion limitations of L-arginine across the unstirred pericellular aqueous layer and the lipid bilayer. Nevertheless, owing to the exceptional preservation of k_{cat}, the overall k_{cat}/K_M of cell-associated liposomal arginase remained 2.6-fold superior to that of the native enzyme (Table 7).

Table 7. Kinetic parameters of arginase activity in homogeneous buffer solution and directly on LLC1 cells obtained via FTIR spectroscopy. Data are presented as mean ± SD. Cell-associated activity was measured after 6 h of incubation with LLC1 cells followed by separation of unbound enzyme (2×, 500 g, 10 min). The percentage of enzyme binding to LLC1 cells was determined fluorometrically (515/550) using arginase covalently labeled with eosin isothiocyanate. The kinetic parameters were calculated using non-linear least-squares fitting of the full product accumulation curves to the differential rate equation incorporating competitive product inhibition. The initial substrate concentration was $[S]_0$ = 20 mM. The catalytic constant was calculated assuming a monomer molecular weight of ~35 kDa for arginase.

Group	Parameter	Native Arginase	Liposomal Arginase
In buffer	**K_M, mM**	3.60 ± 0.25	3.65 ± 0.27
	Specific activity, IU/mg	473 ± 21	429 ± 19
	k_{cat}, s^{-1}	276 ± 12	250 ± 11
	k_{cat}/K_M, $s^{-1}\times M^{-1}$	$(7.6 \pm 0.6) \times 10^4$	$(6.8 \pm 0.5) \times 10^4$
On LLC1 cells	**Binding to LLC1 cells, %**	7 ± 1	15 ± 3
	Observed specific activity, IU/mg	9.0 ± 0.8	57.5 ± 1.2
	Specific activity (per bound protein), IU/mg	128.6 ± 11.4	383.3 ± 8.0
	K_M, mM	7.2 ± 1.4	8.6 ± 1.1
	k_{cat}, s^{-1}	75.0 ± 6.7	223.6 ± 4.7
	k_{cat}/K_M, $s^{-1}\times M^{-1}$	$(1.0 \pm 0.2) \times 10^4$	$(2.6 \pm 0.3) \times 10^4$

From a broader perspective, the methodology established herein opens entirely new horizons for the rational design, screening, and preclinical validation of targeted drug delivery systems (TDDS) and therapeutic nanoreactors. In the development of targeted nanomedicines, optimizing ligand–receptor affinity and maximizing cellular uptake are only half the battle; it is equally vital to ensure that the therapeutic payload remains catalytically competent after docking to the target cell. Our platform allows researchers to decouple quantitative delivery efficiency from qualitative functional preservation (how well the delivered enzyme works in situ). This provides a powerful predictive filter for engineering next-generation targeted enzyme therapies, ensuring that candidate formulations maintain high catalytic flux directly at the pathological site.

4. Discussion

The development of real-time, reagent-free kinetic assays is critical for advancing therapeutic and diagnostic enzymology. For amino-acid-depleting biologic drugs like arginase, accurate assessment of catalytic activity within complex nanocarriers directly dictates clinical efficacy. Historically, measuring arginase kinetics relied on disruptive, multistep chemical methods. We overcame this fundamental limitation by validating a multimodal spectroscopic platform—utilizing far-UV absorbance, circular dichroism, and Fourier-transform infrared spectroscopy—to directly and continuously monitor L-arginine

hydrolysis. This approach successfully extends our label-free analytical paradigm, previously established for L-asparaginase, directly to the arginase system.

The clinical significance of this continuous methodology extends far beyond formulation screening, as arginase serves as a fundamental disease biomarker. Its expression strictly regulates alternative macrophage activation, making dynamic shifts in arginase activity a primary indicator of the macrophage polarization states that drive the pathogenesis of respiratory and joint disorders. By eliminating the structural interference and artifacts of traditional end-point assays, our real-time optical readout provides a transformative analytical engine for targeted diagnostic platforms designed to profile these specific macrophage populations with unprecedented kinetic resolution.

Furthermore, this direct measurement strategy is absolutely indispensable for the rational design of next-generation delivery systems. Advanced nanocarriers, such as the liposomes evaluated in this study, inherently create formidable optical barriers (turbidity and light scattering) that severely confound standard colorimetric evaluations. Our multimodal approach seamlessly bypasses this lipid interference, allowing us to uncover the profound conformational restriction and long-term thermodynamic stabilization that arginase achieves upon encapsulation. Ultimately, by bridging the gap between structural biophysics and pharmaceutical science, this label-free framework accelerates the development of both highly resilient enzyme therapeutics and precision clinical diagnostics.

4.1. Analytical Sensitivity and the Selection of Spectroscopic Modalities

The establishment of any novel kinetic assay necessitates a rigorous evaluation of its analytical figures of merit (Table 8). The selection of an appropriate spectroscopic technique represents a fundamental trade-off between absolute analytical sensitivity and optical tolerance to the sample matrix.

Our data demonstrate that tracking the reaction via far-UV absorbance at 200 nm provides the highabsolute sensitivity, yielding an LOD of 0.026 ± 0.001 U/mL and an LOQ of 0.085 ± 0.003 U/mL. This extreme sensitivity makes it an ideal choice for evaluating highly purified, low-concentration free enzyme preparations. However, this modality is acutely susceptible to Rayleigh scattering and non-specific deep-UV absorption, strictly limiting its application to perfectly clear, homogenous aqueous solutions.

Far-UV CD spectroscopy offers an intermediate sensitivity profile (LOD 0.31 ± 0.02 U/mL) but introduces a critical structural dimension. Unlike simple scalar absorbance, CD provides vector-like chiral information. Monitoring the ellipticity change at 205 nm allows for the direct tracking of the chiral perturbation induced by the hydrolytic cleavage of the bulky guanidinium group. More importantly, CD establishes a dual-modality analytical platform: the identical instrument and sample setup can be utilized to seamlessly transition from assessing the kinetic function of the enzyme to evaluating its thermal stability and secondary structure preservation.

Conversely, ATR-FTIR spectroscopy exhibited the highest LOD among the three methods (0.47 ± 0.05 U/mL). However, this apparent limitation in absolute sensitivity is entirely offset by its unparalleled tolerance for highly scattering, turbid media, a characteristic that becomes indispensable when analyzing encapsulated therapeutics.

Table 8. Limits of detection (LOD) and quantification (LOQ) of arginase activity under substrate-saturating conditions.

Figure of Merit	CD Spectroscopy	Absorbance (200 nm)	FTIR Spectroscopy
LOD, U/mL	0.31 ± 0.02	0.026 ± 0.001	0.47 ± 0.05
LOQ, U/mL	1.05 ± 0.07	0.085 ± 0.003	1.57 ± 0.17

4.2. Overcoming the Limitations of Classical and Discontinuous Assays

A critical comparison with existing methodologies (Table 9) reveals the profound methodological advantages of the spectroscopic techniques proposed herein. Historically, the evaluation of arginase kinetics has depended on destructive, end-point chemical derivatizations. For example, the Sakaguchi reaction [19] and the p-nitrophenylglyoxal assay [20] quantify residual arginine but suffer from narrow dynamic ranges, variable color yields, and the harsh oxidative degradation of the target molecules. Similarly, assays designed to detect the reaction products, such as the ninhydrin method for L-ornithine [23,24] or the diacetyl monoxime assay for urea [21,22], require aggressive stopping steps involving extreme heat (boiling) and highly concentrated acids. These severe conditions instantly denature the enzyme, fundamentally precluding real-time kinetic monitoring and requiring labor-intensive, multi-tube setups simply to reconstruct a single kinetic progress curve.

While continuous reaction monitoring can theoretically be achieved using the Ozer coupled-enzyme assay [25] or potentiometric and pH-stat titrations [26], these approaches introduce significant new vulnerabilities. Coupled assays rely on a fragile cascade of auxiliary enzymes (urease and glutamate dehydrogenase) and expensive cofactors, making them highly susceptible to false readouts caused by matrix components inhibiting the secondary enzymes rather than the arginase itself. Potentiometric methods, though continuous, track secondary bulk-solution phenomena (proton fluxes or ammonium generation) rather than the direct primary cleavage of the substrate, and frequently suffer from sensor fouling. In stark contrast, our CD and FTIR approaches track the primary chemical event—the hydrolysis of the L-arginine guanidinium group—in real-time, in a single measurement run, and completely without the addition of exogenous chemical reagents or enzymatic cascades.

Table 9. Comparative overview of methods for determining arginase activity.

Method (Class)	Detection Principle	Reagents/Conditions	Stopping Step	Typical Analysis Time per Data Point	Sensitivity/Detection Range	Real-Time	Applicability in Optically Dense Media	Key Limitation
Sakaguchi (residual arginine) [19]	Guanidinium + hypobromite/1-naphthol → colored adduct, Abs ~500 nm	NaOBr, 1-naphthol/8-hydroxyquinoline	Yes	~10–30 min color development	Qualitative to semi-quantitative; slow, variable color yield	No	Poor	Classical reaction is inherently non-quantitative; guanidinium groups partly destroyed by the oxidant
p-Nitrophenylglyoxal (residual arginine) [20]	Arginine + p-nitrophenylglyoxal/ascorbate → chromophore, Abs 475 nm	p-Nitrophenylglyoxal, Na-ascorbate	Yes	~30 min at pH 9.0, 30 °C	Linear 0.03–0.33 mM arginine	No	Poor	Endpoint-only; narrow linear range; alkaline incubation step
Ninhydrin/Chinard (L-ornithine) [23,24]	Ornithine + ninhydrin → chromophore, Abs ~515 nm	Ninhydrin reagent, heating step	Yes	~15–60 min per plate/tube	Detection limit ~0.02 µmol urea equivalent (microplate variant)	No	Poor	Endpoint assay; multiple tubes/wells needed to reconstruct a rate; ninhydrin also reacts with free amines/contaminating amino acids
Diacetyl monoxime (product, urea) [21,22]	Urea + diacetyl monoxime (strong acid, heat) → diazine chromophore, Abs ~540 nm	Diacetyl monoxime, strong acid, heat	Yes	~20–30 min heating step	Sub-mM urea, method-dependent	No	Poor	Requires strong acid/heat; interference from ammonia and other reactive nitrogen species
Ozer coupled-enzyme assay (product, urea→NH_4^+) [25]	Arginase → urease → glutamate dehydrogenase; NAD(P)H oxidation followed at 340 nm	Urease, glutamate dehydrogenase, NAD(P)H, 2-oxoglutarate	No (continuous spectrophotometric)	Continuous monitoring, ~5–10 min per run	Linear 0.06–0.30 U/0.5 mL	Yes	Poor	Requires two auxiliary enzymes and a cofactor; cross-reactivity/inhibition by sample matrix components affecting urease or GDH

Potentiometric/ISE and pH-stat (product, NH_4^+/H^+) [26]	Urease-generated NH_4^+ detected by ion-selective electrode, or H^+ release followed by pH-stat titration	Urease (biosensor), titrant	No	Continuous, ~5–15 min per run	Sub-mM to mM range, electrode-dependent	Yes	Moderate (electrode largely insensitive to turbidity)	Electrode drift/fouling; indirect (reports urease/proton chemistry, not arginine/ornithine directly)
Far-UV CD, this work (native substrate/product, 205 nm)	Direct ellipticity of L-Arg vs. L-Orn	None (label-free)	No	Continuous, single run (~5–30 min total)	LOD 0.31 ± 0.02 U/mL; LOQ 1.05 ± 0.07 U/mL	Yes	Poor–moderate (requires optically clear, low-scattering sample)	Lower sensitivity than absorbance; CD signal of the enzyme itself can superimpose on substrate/product bands
Far-UV absorbance, this work (native substrate/product, 200 nm)	Direct UV absorbance of L-Arg vs. L-Orn	None (label-free)	No	Continuous, single run	LOD 0.026 ± 0.001 U/mL; LOQ 0.085 ± 0.003 U/mL	Yes	Poor	Requires optically clear sample; not usable directly on liposomal suspensions
ATR-FTIR, this work (native substrate/product, 1630–1675 cm^{-1} guanidinium band)	Direct mid-IR absorbance of the arginine guanidinium doublet vs. the ornithine carboxylate/ammonium envelope	None (label-free)	No	Continuous, single run (~5–30 min total)	LOD 0.47 ± 0.05 U/mL; LOQ 1.57 ± 0.17 U/mL	Yes	Good	Lower sensitivity than absorbance

4.3. ATR-FTIR: Resolving the Analytical Bottleneck in Nanomedicine Formulation

The most formidable analytical bottleneck in the contemporary development of therapeutic enzymes lies in evaluating their activity once encapsulated within complex, highly turbid drug delivery vehicles. Both conventional UV absorbance and far-UV CD methodologies degrade entirely in the presence of intact liposomal suspensions due to overwhelming optical scattering and non-specific lipid absorption. We previously encountered this exact methodological barrier during our investigations into liposomal, conjugated and nanogel L-asparaginase formulations, where standard spectrophotometric Nesslerization assays proved completely unviable without first aggressively lysing the lipid vesicles to extract the enzyme [28,31,32].

In the present study, ATR-FTIR spectroscopy successfully bypasses this barrier, emerging as an exceptionally robust analytical tool for heterogeneous media. By continuously monitoring the decay of the substrate-specific guanidinium vibrational bands (1630–1675 cm^{-1}) and the concomitant rise in the ornithine-specific modes, we successfully generated high-resolution kinetic profiles for the encapsulated enzyme without any sample pre-treatment. The physical basis for this success lies in the ATR geometry itself: the infrared beam generates an evanescent wave that penetrates only a few micrometers into the sample in contact with the internal reflection element. Consequently, it measures the localized chemical composition at the interface while remaining nearly entirely blind to the bulk optical scattering that confounds transmission techniques. This distinct optical property allowed us to directly and continuously monitor the catalytic turnover of arginase in situ within the optically dense phosphatidylcholine/cardiolipin suspension. The kinetic data confirmed that the intact phospholipid boundary permits unimpeded substrate influx and product efflux, preserving ~90% of the native enzyme's catalytic efficiency.

Ultimately, the integration of far-UV absorbance, CD, and ATR-FTIR spectroscopy provides a comprehensive, label-free analytical toolkit that addresses the full spectrum of arginase research requirements. While UV absorbance provides ultimate sensitivity for purified systems, and CD uniquely bridges kinetic function with thermodynamic structural analysis, ATR-FTIR provides a critical breakthrough for the evaluation of turbid,

next-generation nanomedicines. By eliminating the reliance on destructive chemical derivatization, these continuous spectroscopic methods significantly streamline the biochemical evaluation of antineoplastic enzymes, accelerating the crucial transition from fundamental biophysical engineering to advanced preclinical formulation.

4.4. Liposomal Arginase Formulation

While liposomal arginase undergoes a qualitatively similar structural transition—marked by a reduction in the alpha-helix fraction from 20% to 14.6%—the overall amplitude of this unfolding event is profoundly attenuated. Across all temperatures exceeding 50 °C, the encapsulated enzyme consistently retains 3 to 4 percentage points more helical content than its free counterpart, indicating that the lipid bilayer imposes strict conformational constraints on the protein architecture. This restricted mobility is quantitatively reflected in the unfolding equilibrium constant (K = [D]/[N], representing the ratio of denatured to native protein fractions) and the subsequent van't Hoff analysis. Under severe thermal stress at 80 °C, the free enzyme reaches an equilibrium constant of K = 0.7, signifying a substantial population shift toward the denatured state. In striking contrast, the unfolding trajectory of lipo-ARG reaches a premature plateau at K = 0.4. By remaining well below unity, this value definitively proves that the native, folded conformation persists as the dominant state even at extreme temperatures, effectively rendering global denaturation thermodynamically inaccessible.

The thermodynamic parameters further illuminate this stabilization mechanism. Upon encapsulation, the enthalpy of unfolding ΔH experiences a nearly threefold increase, escalating from 156 to 466 kJ/mol. This immense energetic penalty is elegantly offset by a proportionally larger entropy gain (ΔS), which rises from 467 to 1400 J/(mol K) (Table 6). Such robust enthalpy-entropy compensation serves as the classic thermodynamic hallmark of a cooperative, multipoint lipid-protein interface. To unfold the encapsulated arginase, the system must simultaneously sever a vast network of strong protein-lipid interactions. This collective rupture drives the massive enthalpic cost while concurrently liberating an abundance of structural degrees of freedom, explaining the profound entropic surge. As a result, the net free-energy barrier and the apparent melting temperature (Tm) exhibit a far more moderate shift than the drastic isolated change in ΔH would otherwise predict.

5. Conclusions

Evaluating amino-acid-depleting enzymes is traditionally bottlenecked by indirect, discontinuous assays. To overcome this limitation, we established two robust, reagent-free spectroscopic methods—circular dichroism (CD, 205 nm) and attenuated total reflectance Fourier-transform infrared (ATR-FTIR, ~1630–1675 cm^{-1}) spectroscopy—that directly and continuously track L-arginine hydrolysis, completely eliminating the need for harsh stopping reagents or fragile coupled-enzyme cascades. The developed methods proved highly sensitive, achieving LOD of 0.026 U/mL and maintaining high analytical precision across both free and liposome-encapsulated formulations.

Applying this analytical platform to a highly light-scattering liposomal arginase formulation revealed that physical encapsulation within a phosphatidylcholine/cardiolipin bilayer preserves approximately 90% of the native enzyme's catalytic efficiency (k_{cat}/K_M = 6.8×10^4 $M^{-1} \cdot s^{-1}$ vs 7.6×10^4 $M^{-1} \cdot s^{-1}$ for the free enzyme). Crucially, the lipid nanocarrier significantly increases the enzyme's functional persistence under acute thermal stress. By shifting the inactivation profile, the liposomal formulation prevents irreversible macroscopic aggregation and drives the inactivation kinetics toward a stable, resilient plateau, achieving a terminal residual activity of 70% after 60 min at 55 °C, compared to 62% for the free enzyme.

https://doi.org/10.3390/analytica7040088

Thermodynamic and kinetic evaluations elucidated the molecular factors driving this substantial stabilization. While the free enzyme undergoes initial structural unfolding that progressively triggers intermolecular aggregation, the encapsulated enzyme retains 40–50% of its native secondary architecture even at extreme temperatures (80 °C). Analysis of the CD melting thermograms enabled a quantitative comparison of the apparent thermodynamic parameters governing the conformational transitions of the liposomal formulation and the native enzyme. Spatial confinement and protective association within the liposomal nanostructure effectively restrict intermolecular collisions and induce a substantial enthalpic barrier to thermal denaturation, raising the apparent unfolding enthalpy $\Delta_{unf}H$ from 156 to 466 kJ/mol. This structural protection directly translates into the observed sustained catalytic activity.

Most importantly, bypassing the optical scattering limitations of whole-cell suspensions via ATR-FTIR spectroscopy allowed us for the first time to bridge the gap between idealized in vitro solutions and the complex cellular interface by determining steady-state enzymatic kinetics directly on LLC1 cells. Coupling fluorometric binding assays with in situ FTIR kinetic profiling revealed a critical dual benefit of liposomal delivery: encapsulation acted as a protective molecular shield against surface-induced inactivation. Whereas naked cell-bound arginase suffered a drastic loss of function—retaining only ~27% of its intrinsic turnover rate (k_{cat} dropping from 276 s^{-1} in buffer to 75 s^{-1} on cells)—cell-associated liposomal arginase preserved ~90% of its native catalytic turnover (k_{cat} = 223.6 s^{-1}), yielding a 6.4-fold higher specific activity (57.5 vs. 9.0 IU/mg) and a 2.6-fold superior catalytic efficiency directly on the target cell surface.

The pharmacological and bioanalytical implications of these findings are substantial, given the emerging role of arginase in both oncology and immunology. While the direct deployment of these methods for clinical biomarker profiling in unpurified blood and tissue samples represents a future direction requiring adaptation to physiological pH, the developed spectroscopic platform is highly promising for immediate application in the preclinical optimization of next-generation arginase nanomedicines. By enabling researchers to decouple quantitative cellular accumulation from qualitative in situ functional preservation and rapidly confirming that liposomal encapsulation enhances structural stability, thermal resilience, and target-cell retention without sacrificing catalytic turnover. This methodology establishes a new paradigm for validating targeted drug delivery systems and significantly accelerates the rational design of long-acting enzyme therapeutics.

Author Contributions: Conceptualization, E.V.K. and I.D.Z.; methodology, I.D.Z., P.I.N. and E.V.K.; formal analysis, I.D.Z.; investigation, I.D.Z., P.I.N. and E.V.K.; data curation, I.D.Z.; writing—original draft preparation, I.D.Z.; writing—review and editing, E.V.K.; project supervision, E.V.K.; funding acquisition, E.V.K. All authors have read and agreed to the published version of the manuscript.

Funding: This research received no external funding.

Data Availability Statement: The original contributions presented in this study are included in the article. Further inquiries can be directed to the corresponding author.

Acknowledgments: This work was performed using the equipment FTIR microscope MICRAN-3 (Simex, Novosibirsk, Russia), Jasco J-815 CD Spectrometer (JASCO, Tokyo, Japan), AFM microscope NTEGRA II (NT-MDT Spectrum Instruments, Moscow, Russia), and confocal laser scanning microscope FluoView FV1000 (Olympus, Tokyo, Japan) of the program of Moscow State University development.

Conflicts of Interest: The authors declare no conflicts of interest.

References

1. Mortier, J.; Prévost, J.R.C.; Sydow, D.; Teuchert, S.; Omieczynski, C.; Bermudez, M.; Frédérick, R.; Wolber, G. Arginase Structure and Inhibition: Catalytic Site Plasticity Reveals New Modulation Possibilities. *Sci. Rep.* **2017**, *7*, 13616. https://doi.org/10.1038/s41598-017-13366-4.
2. Durante, W.; Johnson, F.K.; Johnson, R.A. Arginase: A Critical Regulator of Nitric Oxide Synthesis and Vascular Function. *Clin. Exp. Pharmacol. Physiol.* **2007**, *34*, 906–911. https://doi.org/10.1111/j.1440-1681.2007.04638.x.
3. Ash, D.E. Structure and Function of Arginases. *J. Nutr.* **2004**, *134*, 2760S–2764S. https://doi.org/10.1093/jn/134.10.2760S.
4. Christianson, D.W. Arginase: Structure, Mechanism, and Physiological Role in Male and Female Sexual Arousal. *Acc. Chem. Res.* **2005**, *38*, 191–201. https://doi.org/10.1021/ar040183k.
5. Marzęta-Assas, P.; Jacenik, D.; Zasłona, Z. Pathophysiology of Arginases in Cancer and Efforts in Their Pharmacological Inhibition. *Int. J. Mol. Sci.* **2024**, *25*, 9782. https://doi.org/10.3390/ijms25189782.
6. Li, M.; Qin, J.; Xiong, K.; Jiang, B.; Zhang, T. Review of Arginase as a Promising Biocatalyst: Characteristics, Preparation, Applications and Future Challenges. *Crit. Rev. Biotechnol.* **2022**, *42*, 651–667. https://doi.org/10.1080/07388551.2021.1947962.
7. Li, Z.; Wang, L.; Ren, Y.; Huang, Y.; Liu, W.; Lv, Z.; Qian, L.; Yu, Y.; Xiong, Y. Arginase: Shedding Light on the Mechanisms and Opportunities in Cardiovascular Diseases. *Cell Death Discov.* **2022**, *8*, 1–14. https://doi.org/10.1038/s41420-022-01200-4.
8. Ino, Y.; Yamazaki-itoh, R.; Oguro, S.; Shimada, K.; Kosuge, T.; Zavada, J.; Kanai, Y.; Hiraoka, N. Arginase II Expressed in Cancer-Associated Fibroblasts Indicates Tissue Hypoxia and Predicts Poor Outcome in Patients with Pancreatic Cancer. *PLoS ONE* **2013**, *8*, e55146. https://doi.org/10.1371/journal.pone.0055146.
9. Porembska, Z.; Luboiński, G.; Chrzanowska, A.; Mielczarek, M.; Magnuska, J.; Barańczyk-Kuźma, A. Arginase in Patients with Breast Cancer. *Clin. Chim. Acta* **2003**, *328*, 105–111. https://doi.org/10.1016/S0009-8981(02)00391-1.
10. Kaysen, G.A.; Strecker, H.J. Purification and Properties of Arginase of Rat Kidney. *Biochem. J.* **1973**, *133*, 779–788. https://doi.org/10.1042/bj1330779.
11. Heuser, S.K.; Li, J.; Pudewell, S.; LoBue, A.; Li, Z.; Cortese-Krott, M.M. Biochemistry, Pharmacology, and in Vivo Function of Arginases. *Pharmacol. Rev.* **2025**, *77*, 100015. https://doi.org/10.1124/pharmrev.124.001271.
12. Dowling, D.P.; Ilies, M.; Olszewski, K.L.; Portugal, S.; Mota, M.M.; Llinás, M.; Christianson, D.W. Crystal Structure of Arginase from Plasmodium Falciparum and Implications for l -Arginine Depletion in Malarial Infection. *Biochemistry* **2010**, *49*, 5600–5608. https://doi.org/10.1021/bi100390z.
13. Sekula, B. The Neighboring Subunit Is Engaged to Stabilize the Substrate in the Active Site of Plant Arginases. *Front. Plant Sci.* **2020**, *11*, 1–12. https://doi.org/10.3389/fpls.2020.00987.
14. Mudedla, S.K.; Ghosh, B.; Dhoke, G.V.; Oh, S.; Wu, S. QM/MM Simulations for the Broken-Symmetry Catalytic Reaction Mechanism of Human Arginase I. *ACS Omega* **2022**, *7*, 32536–32548. https://doi.org/10.1021/acsomega.2c04116.
15. Changou, C.A.; Chen, Y.R.; Xing, L.; Yen, Y.; Chuang, F.Y.S.; Cheng, R.H.; Bold, R.J.; Ann, D.K.; Kung, H.J. Arginine Starvation-Associated Atypical Cellular Death Involves Mitochondrial Dysfunction, Nuclear DNA Leakage, and Chromatin Autophagy. *Proc. Natl. Acad. Sci. USA* **2014**, *111*, 14147–14152. https://doi.org/10.1073/pnas.1404171111.
16. Sparkes, R.S.; Dizikes, G.J.; Klisak, I.; Grody, W.W.; Mohandas, T.; Heinzmann, C.; Zollman, S.; Lusis, A.J.; Cederbaum, S.D. The Gene for Human Liver Arginase (ARG1) Is Assigned to Chromosome Band 6q23. *Am. J. Hum. Genet.* **1986**, *39*, 186–193.
17. Cheng, P.N.M.; Lam, T.L.; Lam, W.M.; Tsui, S.M.; Cheng, A.W.M.; Lo, W.H.; Leung, Y.C. Pegylated Recombinant Human Arginase (RhArg-Peg5,000mw) Inhibits the in Vitro and in Vivo Proliferation of Human Hepatocellular Carcinoma through Arginine Depletion. *Cancer Res.* **2007**, *67*, 309–317. https://doi.org/10.1158/0008-5472.CAN-06-1945.
18. Stone, E.M.; Glazer, E.S.; Chantranupong, L.; Cherukuri, P.; Breece, R.M.; Tierney, D.L.; Curley, S.A.; Iverson, B.L.; Georgiou, G. Replacing Mn 2+ with Co 2+ in Human Arginase I Enhances Cytotoxicity toward l -Arginine Auxotrophic Cancer Cell Lines. *ACS Chem. Biol.* **2010**, *5*, 333–342. https://doi.org/10.1021/cb900267j.
19. Loeb, W.F.; Stuhlman, R.A. A Colorimetric Method for the Determination of Serum Arginase Activity. *Clin. Chem.* **1969**, *15*, 162–169. https://doi.org/10.1093/clinchem/15.2.162.
20. Aminlari, M. A Novel Colorimetric Method for Assaying Arginase Activity. *Clin. Biochem.* **1992**, *25*, 431–436. https://doi.org/10.1016/0009-9120(92)90060-6.
21. Langenfeld, N.J.; Payne, L.E.; Bugbee, B. Colorimetric Determination of Urea Using Diacetyl Monoxime with Strong Acids. *PLoS ONE* **2021**, *16*, e0259760. https://doi.org/10.1371/journal.pone.0259760.
22. Satoh, P.S.; Ito, Y. Quantitative Rapid Microassay of Arginase. *Anal. Biochem.* **1968**, *23*, 219–229. https://doi.org/10.1016/0003-2697(68)90353-9.

23. Iyamu, E.W.; Asakura, T.; Woods, G.M. A Colorimetric Microplate Assay Method for High-Throughput Analysis of Arginase Activity in Vitro. *Anal. Biochem.* **2008**, *383*, 332–334. https://doi.org/10.1016/j.ab.2008.08.016.
24. Smith, N.J.; Maddahfar, M.; Gunasegaran, B.; McGuire, H.M.; Fazekas de St Groth, B. A High-Throughput Colorimetric Microplate Assay for Determination of Plasma Arginase Activity. In *Methods in Molecular Biology*; Springer: New York, NY, USA, 2023; Volume 2620, pp. 273–286, ISBN 9781071629413.
25. Özer, N. A New Enzyme-Coupled Spectrophotometric Method for the Determination of Arginase Activity. *Biochem. Med.* **1985**, *33*, 367–371. https://doi.org/10.1016/0006-2944(85)90012-2.
26. Urbanowicz, M.; Sadowska, K.; Paziewska-Nowak, A.; Sołdatowska, A.; Pijanowska, D.G. Biosensor Based on Coupled Enzyme Reactions for Determination of Arginase Activity. *Bioelectrochemistry* **2022**, *146*, 108137. https://doi.org/10.1016/j.bioelechem.2022.108137.
27. Dabrowska, A.; Schwaighofer, A.; Lendl, B. Mid-Infrared Dispersion Spectroscopy as a Tool for Monitoring Time-Resolved Chemical Reactions on the Examples of Enzyme Kinetics and Mutarotation of Sugars. *Appl. Spectrosc.* **2024**, *78*, 982–992. https://doi.org/10.1177/00037028241258109.
28. Zlotnikov, I.D.; Kudryashova, E.V. A Novel Approach for the Activity Assessment of L-Asparaginase Formulations When Dealing with Complex Biological Samples. *Int. J. Mol. Sci.* **2025**, *26*, 5227. https://doi.org/10.3390/ijms26115227.
29. Kudryashova, E.V.; Pokrovskaya, M.V.; Alexandrova, S.S.; Vinogradov, A.A.; Sokolov, N.N. FTIR-Based L-Asparaginase Activity Assay Enables Continuous Measurements in Optically Dense Media Including Blood Plasma. *Anal. Biochem.* **2020**, *598*, 113694. https://doi.org/10.1016/j.ab.2020.113694.
30. Spector, E.B.; Rice, S.C.H.; Moedjono, S.; Bernard, B.; Cederbaum, S.D. Biochemical Properties of Arginase in Human Adult and Fetal Tissues. *Biochem. Med.* **1982**, *28*, 165–175. https://doi.org/10.1016/0006-2944(82)90067-9.
31. Zlotnikov, I.D.; Shishparyonok, A.N.; Pokrovskaya, M.V.; Alexandrova, S.S.; Zhdanov, D.D.; Kudryashova, E. V Structural Features Underlying the Mismatch Between Catalytic and Cytostatic Properties in L-Asparaginase from Rhodospirillum Rubrum. *Catalysts* **2025**, *15*, 476. https://doi.org/10.3390/catal15050476.
32. Zlotnikov, I.D.; Ezhov, A.A.; Kudryashova, E.V. Receptor-Mediated Internalization of L-Asparaginase into Tumor Cells Is Suppressed by Polyamines. *Int. J. Mol. Sci.* **2025**, *26*, 6749. https://doi.org/10.3390/ijms26146749.

Disclaimer/Publisher's Note: The statements, opinions and data contained in all publications are solely those of the individual author(s) and contributor(s) and not of MDPI and/or the editor(s). MDPI and/or the editor(s) disclaim responsibility for any injury to people or property resulting from any ideas, methods, instructions or products referred to in the content.